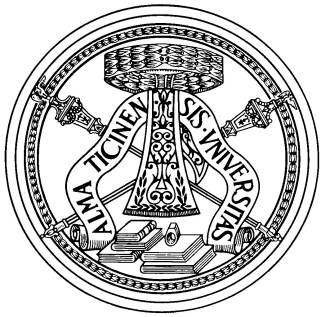

UNIVERSITY OF PAVIA

FACULTY OF ENGINEERING

CIVIL ENGINEERING AND ARCHITECTURE DEPARTMENT

MASTER'S DEGREE IN BIOENGINEERING

3D PRINTING OF PCL SCAFFOLDS REINFORCED WITH HYDROXYAPATITE FOR BONE TISSUE REGENERATION

Scaffold di PCL rinforzato con idrossiapatite per rigenerazione ossea ottenuti mediante 3D printing

Candidate: Pierpaolo Fucile - 443294

Supervisor:	Prof. Michele Conti
Co-supervisors:	Prof. Ferdinando Auricchio
	Prof. Antonio Gloria

Academic year 2016/2017

"I felt like this on my way home, I'm not scared"

[D. Grohl]

A Elda e Rita

Abstract

Additive Manufacturing (AM) techniques, such as Fused Deposition Modelling and 3D Bioprinting, which allows to create 3D biocompatible scaffolds on which cells can be seeded, represent a breakthrough for tissue engineering, especially in the field of bone tissue regeneration, being a promising alternative to autogenous bone grafting, which may be difficult due to several reasons, such as the shaping process or, in case of other sources, immuno-rejection.

The present work aims at designing and realizing scaffolds for bone tissue engineering, using AM techniques. Materials were chosen according to bone's ECM composition, which shows both organic and inorganic phase: polycaprolactone (PCL) was chosen as the polymeric matrix of the compound, thanks to its biocompatibility, bioactivity and *controllable* biodegradability, so to replace bone functions for all the regeneration process; hydroxyapatite (HA) was chosen as organic reinforcement, because it is the mineral phase of bone's ECM itself. Plain PCL scaffolds were realized as control.

The work is part of a collaboration between the University of Pavia, (Computational Mechanics and Advanced Group), and the *Istituto per i Polimeri Compositi e Biomateriali - Consiglio Nazionale delle Ricerche* (IPCB-CNR) in Naples.

A commercial 3D bioplotter, the Cellink INKREDIBLE+, was used. It is a pneumatic-based printer, which allows to print hydrogels and polymeric pellets. It is located in the Experimental Surgery Laboratory at the University of Pavia, providing ideal environment to guarantee samples sterility.

The first part of this work deals with the PCL printing characterization, which consists in the measurement of PCL strands diameter that different pressure and extrusion speed values provide. In particular, three values for each were chosen, and three different printer's nozzles were selected (0.3 mm, 0.5 mm, and 0.7 mm nozzle diameter). After a pressure was set, three stripes, one for each extrusion speed value, were printed and photographed. Every

test was conducted three times due to statistical ends: this means 9 tests for each nozzle were conducted, for a total of 27 tests. The results of such analysis suggested the printing parameters used to manufacture cylindrical scaffolds with a diameter of 6 mm. They were 46 in total, 23 for each material, and their height depended on the type of analysis they were subject to: 6 mm for compression tests, and 2 mm for biological analysis, which consisted in cells seeding (human mesenchymal stem cells) and viability tests, measured via Alamar Blue Assay, which is a colorimetric redox indicator that changes colour as cells proliferate. Serum's colour change is linked to the Alamar Blue's reduction, and so to the number of viable cells. Measurements were carried out after 1, 3, and 7 days after cells seeding. All those tests were conducted in Naples.

Results showed how plain PCL is not suitable for bone tissue engineering. It lacks mechanical properties: for a same induced deformation level, 50%, PCL/HA scaffolds' sustainable stress is 11 MPa, while it is only 4.5 MPa for the plain PCL ones. Even compressive modulus was higher for the reinforced samples. Hydroxyapatite causes hardening in the structure, allowing the scaffold to sustain higher stresses. Alamar Blue reduced circa 10% more in reinforced scaffolds' serum: this means more cells were viable.

Our work proved that for bone tissue engineering, PCL needs a reinforcement, and hydroxyapatite, bone's mineral phase, is one of the best choices. Our results are coherent with literature's ones (e.g., works made by *Gloria* in 2013, and by *Park* in 2011), as well as with CNR laboratory experience.

Sommario

Le tecniche di Additive Manufacturing (AM), come la Fused Deposition Modelling (FDM) ed il 3D Bioprinting, che permettono di creare scaffold 3D biocompatibili su cui poter seminare le cellule, rappresentano una svolta nell'ingegneria tissutale, specialmente nel campo della rigenerazione ossea, in quanto sono una promettente alternativa all'autotrapianto osseo che alcune variabili, come il processo di modellamento o il rigetto immunitario nel caso di donatore, possono rendere difficile.

Il seguente lavoro punta a progettare e realizzare degli scaffold per l'ingegneria tissutale del tessuto osseo, utilizzando tecniche AM. I materiali sono stati scelti rispettando la composizione della matrice extracellulare dell'osso, che mostra sia una parte organica sia inorganica: il policaprolattone (PCL) è stato scelto come matrice polimerica del materiale composito, grazie alla sua biocompatibilità, bioattività e biodegradabilità *controllata*, così da poter sostituire le normali funzioni dell'osso durante il processo rigenerativo; l'idrossiapatite (HA) è stata scelta come rinforzo organico, poiché è parte della fase minerale della ECM dell'osso. Sono stati, inoltre, realizzati scaffold in PCL non caricato come controllo.

Il lavoro è nato da una collaborazione tra l'Università di Pavia (Computational Mechanics and Advanced Group) e l'*Istituto per i Polimeri Compositi e Biomateriali - Consiglio Nazionale delle Ricerche* (IPCB-CNR) di Napoli.

E' stato utilizzato un Bioplotter 3D commerciale, il Cellink INKREDIBLE+: si tratta di una stampante a estrusione pneumatica, che permette di stampare hydrogel e pellets polimerici. E' situata nel laboratorio di Chirurgia Sperimentale dell'Università di Pavia, in modo da garantire un ambiente sterile per i campioni.

La prima parte di questo lavoro è rappresentata dalla caratterizzazione della stampa del PCL, che consiste nella misurazione del diametro dei filamenti prodotti da diverse coppie di valori di pressione e velocità di stampa. In particolare sono stati scelti tre valori per

ognuna e tre diversi estrusori di stampa (con un diametro dell'ugello di 0.3 mm, 0.5 mm e 0.7 mm). Dopo aver fissato una pressione, sono state stampate e fotografate tre strisce, una per ogni valore di velocità di estrusione. Ogni test è stato condotto tre volte per fini statistici: quindi 9 test per ogni estrusore, per un totale di 27 test. I risultati di questa analisi hanno suggerito i parametri di stampa utilizzati per realizzare scaffold cilindrici con un diametro di 6 mm. In totale sono 46, 23 per ogni materiale, e la loro altezza dipende dal tipo di analisi a cui sono stati sottoposti: 6 mm per i test di compressione, mentre 2 mm per le analisi biologiche, che consistono in una semina cellulare (cellule staminali mesenchimali umane) e in un test di viabilità, misurata attraverso il saggio dell'Alamar Blue, che è un indicatore redox colorimetrico che cambia colore quando le cellule proliferano. Il cambiamento di colore del siero è collegato alla riduzione dell'Alamar Blue e, quindi, al numero di cellule vitali. Le misurazioni sono state condotte a 1, 3 e 7 giorni dopo la semina cellulare. Tutti questi test sono stati condotti a Napoli.

I risultati hanno mostrato come il PCL scarico non sia adatto per applicazioni di ingegneria tissutale ossea. Le sue proprietà meccaniche sono scarse: a parità di livello di deformazione indotta, 50%, lo sforzo sostenibile dagli scaffold in PCL/HA è di 11 MPa, mentre è solo 4.5 MPa per quelli di PCL scarico. Anche il modulo a compressione è risultato più elevato per i campioni rinforzati. L'idrossiapatite causa un indurimento della struttura, permettendo allo scaffold di sostenere sforzi maggiori. La riduzione dell'Alamar Blue è risultata maggiore del 10% nel siero degli scaffold rinforzati: ciò vuol dire che più cellule erano vitali.

Il nostro lavoro ha dimostrato che il PCL ha bisogno di un rinforzo per le applicazioni di ingegneria tissutale ossea e l'idrossiapatite, la fase minerale dell'osso, è una delle scelte migliori. I nostri risultati sono coerenti con quelli presenti in letteratura (ad esempio si vedano il lavoro di *Gloria* nel 2013 e di *Park* nel 2011), e con l'esperienza di laboratorio del CNR.

Contents

List of Tables

List of Figures

Chapter 1

Introduction

This thesis deals with *bone tissue engineering* applications. In particular our purpose was to realize biocompatible 3D bioprinted scaffolds made of polycaprolactone reinforced with hydroxyapatite for bone tissue regeneration.

In this chapter, basic principles will be presented, starting from tissue engineering, its applications and fabrication techniques; then, bone tissue, and the best materials used for its regeneration in terms of biocompatibility, osteointegration, biodegradation and mechanical properties. Finally, the state of the art of bone tissue engineering will be reported, and its literature will be reviewed.

1.1 Tissue Engineering

Tissue engineering (TE), also called Regenerative Medicine, is a highly interdisciplinary field, which combines efforts and knowledge from different fields [12], such as biology, engineering, medicine, material science, and genetics. It was first defined in 1988, during the first *National Science Foundation* (NSF) sponsored meeting, as the *"application of principles and methods from engineering and natural science towards the structure-function relationship in healthy and diseased mammalian tissues, and the development of biological substitutes for the repair or regeneration of tissue or organ function"* [13]. Actually, tissue engineering, in its latest definition, is a *"multidisciplinary science which integrates principles of engineering and natural science to develop biological substitutes that can restore, maintain or improve tissue functions"* [14].

Main TE goal is to find a relationship between *structure* and *function*, thus cells will react properly when interacting with a particular material. Another important relationship is the one between cells and the material they are seeded on.

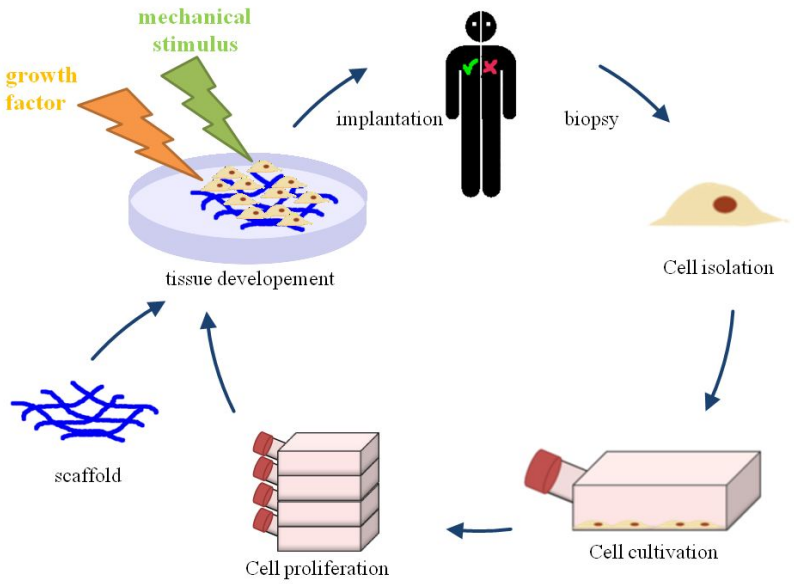

Figure 1.1: Basic principles of Tissue Engineering [2]

Tissue engineering was born to face an important issue, which is the lack of transplantable organs and the very long transplant waiting lists. In addition to that, the traditional approach, which consists in the transplant of biomaterials in the human body, brings with it some risks, such as inflammatory response and a partially restored organ functionality. So, the main aim is to regenerate, instead of replacing.

A standard Tissue Engineering procedure consists on the following experimental steps [15].

1. **Cells:** they are extracted and preserved at low temperatures in liquid nitrogen. *Primary cells* and *stem cells* are used in tissue engineering. The former are extracted via biopsy, they preserve the differentiation parameters of the tissue they were taken from; the latter are not differentiated, differentiation can be induced according to the tissue they are seeded on. Plus, they can divide limitlessly.

2. **Structures:** porous structures are designed, and cells can proliferate into them once seeded. This means an accurate research on biomaterials must be done.

3. **Expansion *in vitro*:** cells must be defrosted and put on a plate inside a laminar flow

cabinet and that is because sterility conditions must be granted. The cabinet provides a descending laminar flow which keeps bacteria away. Another important element is the growth medium: it is liquid and kept at constant and controlled pH values. Different concentrations of calcium ions, vitamins, amino acids and proteins can be found on it. Serum is fundamental, as it contains cellular growth factors.

4. ***In vivo* transplant:** once the porous structure is designed and the cells are seeded into it, it is transplanted inside the body. From that moment, cells start cooperating with the physiological environment and differentiate. This process can be monitored through the application of differentiation markers.

1.1.1 Fabrication approaches to tissue engineering

There are different Tissue Engineering approaches, in different science fields [12, 16]:

- design and growth of human tissues outside the body, for a subsequent transplant;
- taking cells from a donor and seed them directly into the body on specific structures, where they will differentiate and grow, promoting the tissue vascularization (*cell-based therapy*);
- focus on cells - support structure relationship and on stimuli that coordinate tissue regeneration;
- design of external devices which contain human tissues: these are connected to the body, they are not transplanted, so to replace pathological tissues' functions (e.g. artificial liver);
- transplant of devices onto which cells are seeded, so to induce tissue regeneration.

Among the various TE approaches, which range over different applications, lately the term *Biofabrication* (Figure 1.2) emerged with the application of 3D manufacturing strategies [3]. It is defined as "*the automated generation of biologically functional products with structural organization from living cells, bioactive molecules, biomaterials, cell aggregates, through Bio-printing ro Bioassembly and subsequent tissue maturation processes*". This approach aims to be the conjuction between tissue engineering and Additive Manufacturing techniques, as will

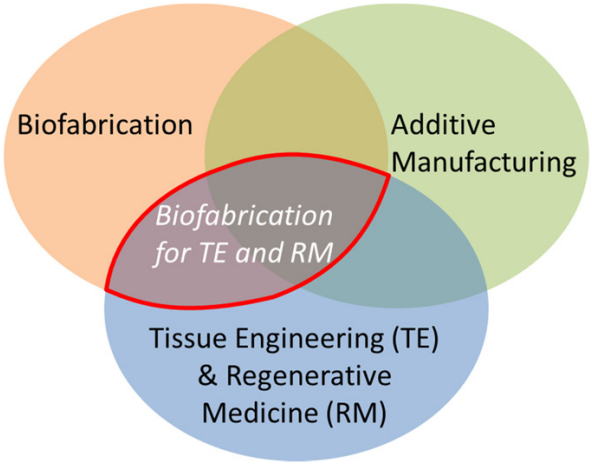

Figure 1.2: Interrelation between Biofabrication, Additive Manufacturing and the TE and RM fields [3]

be discussed in 1.4 and 1.5, and to exploit automated processes to generate cell-biomaterial constructs that may mature into functional tissue equivalents. Bioprinting is one of the two strategies of Biofabrication, together with Bioassembly [3]. These two methods call for a cell seeding and maturation phase, to allow a continuous and coherent functional structure.

Usually, Bioprinting and Biofabrication definitions overlap.

This work can be identified as a biofabrication process, since a bioactive scaffold will be realized for cell seeding and tissue regeneration.

1.2 Scaffolds

The scaffold (Figure 1.3) is a porous polymeric matrix or installation in which cells penetrates into, so to regrow the damaged tissue. Scaffolds can be made of natural or synthetic materials, which temporarily support cells and supervise their growth via cell-material interactions and biologic factor release.

It is possible to recognize different scaffold types [17]:

- *without cells*, causing the regeneration by vascularization, as vessels from surrounding tissues penetrates onto it. This way, the tissue fills and modifies the scaffold, which biodegrades and sustains itself via nutrients supplied by the vessels, such as glucose and oxygen;

- *with cells*, in particular patient's cells that are previously seeded. This way, the scaf-

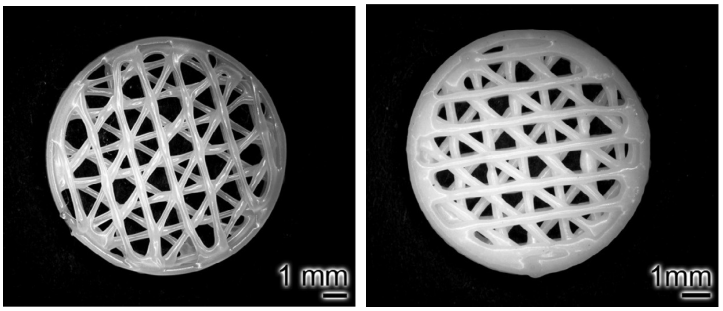

Figure 1.3: Two examples of scaffolds: plain polycaprolactone (PCL) scaffold on the left, PCL/Ca on the right [4]

fold becomes an engineered tissue. In this case there is a complete integration and an expansion from the patient's tissue to scaffold centre and vice versa.

In order to be used in TE, scaffolds must provide the following functions [18]:

- providing a three-dimensional space, so to sustain the regenerating (or forming) tissue;
- supporting cells, allowing their growth, migration, and differentiation;
- promoting tissue's growth, gaining nutrients from surrounding vessels which penetrates into the scaffold;
- it has to temporarily replace tissue's functions (e.g. sustaining loads if the damaged tissue is the bone).

They are essential elements, as they are used to achieve one of tissue engineering's top goals, which is the design of substitutes that grow with the patient [14]. Guidance is guaranteed if the design is compatible with the tissue to be regenerated. According to that, even geometry, materials and matrix architecture must suit the tissue.

So, one of the most challenging goals in TE is designing scaffolds able to guide the tissue regeneration process [18].

1.2.1 Requirements

The ideal scaffold should possess a repertoire of cues (chemical, biochemical, and biophysical) able to control and promote specific events at the cellular and tissue level. In the last decades, the concept of *cell guidance* has been widely discussed [18].

Designing a scaffold means to design nothing but an engineered tissue, since it has to host cells, and these cells has to grow into it, so to regenerate a diseased tissue, or create a new one [12, 17].

Scaffolds have to satisfy the following features [1, 12, 16, 19]:

- **Biocompatibility**: this feature deals with the choice of the material. It must be accepted by the organism and it must not trigger inflammatory response. On the contrary, the material has to be non-toxic, so that the scaffold can moderate the inflammatory response.

- **Biodegradability and Bioresorbability**: these are very important features, since it is crucial for the scaffold to be completely degraded as the tissue is reformed. Degradation time can be *tailored* working on the material composition; it is easy to understand that discordance between degradation and regeneration times could lead to problems: a fast scaffold degradation causes a non-resistant and non-solid tissue, while a slow degradation times results in an incomplete regeneration; once the scaffold degrades, the material it is made of should be processed and expelled, without inflammatory response, like any other organism's waist.

- **Structure**: tissue regeneration is a result of a complex cascade of events, which are coordinated in spatial and temporal modalities, and each of them is governed by biophysical and biochemical signals, triggered by the extracellular microenvironment [18]. Scaffold's structure has to provide spatial stability, so to guide cells onto itself, where they proliferate and produce Extracellular Matrix (*ECM*). The dynamic and reciprocal interaction between cells and ECM is what determines cell fate, ECM degradation or remodelling [20], and other structural properties, such as adhesion, migration and proliferation to a phenotype choice. One of the main features scaffold structure must have is *porosity*, as pores allow the formation of a vascularization network, as well as nutrients transport and metabolic waste removal. Pores must be *interconnected* (highest the interconnection, the better), so to have better adhesion, proliferation, diffusion and penetration. Pores dimension can change with the tissue to regenerate.

- **Mechanical properties**: the scaffold must temporarily replace the tissue and all the functions, especially the mechanical ones, it carried out before the damage. Resistance

and stability are crucial, as well as bearing all the loads tissues bear *in vivo*. There must be a connection between mechanical properties and degradation of the scaffold, meaning that there must be a transition in which the regenerated tissue assumes a greater mechanical role as the scaffold degrades. There is also a *trade-off* between a denser scaffold, which provides greater mechanical properties, and a more porous one, which better interact with cells [18].

- **Bioactivity**: the scaffold must guarantee a connection between the patient's organism and the new tissue.

- **Surface properties**: the ratio of internal surface area and scaffold volume must be high, so that a greater number of cells can be seeded; in addition to that, morphology must be easily moldable (the material must be processable through repeatable processes), and scaffold surface must have chemical properties.

In addition to all those materials and scaffolds properties, a sterile environment must be guaranteed: it is an essential requirement when working with cells, so all the operations must be done using a laminar flow cabinet. It is easy to understand that another requirement is that the scaffold must resist to sterilizing processes. Moreover, an essential requirement scaffolds must have is *sterility*, so to provide cells a suitable environment to grow in and proliferate avoiding contaminations. On the basis of these considerations, all operations must be done using a laminar flow cabinet. Plus, scaffolds must resist to sterilizing processes.

That is why scaffold material selection is a crucial step in scaffold fabrication.

1.2.2 Scaffold's parameters

In Figure 1.4, the most important scaffold's parameters are shown:

- RW, road width, or strand diameter, a combination of pressure and speed;

- FD, filament distance (center to center), or strand distance on the same layer;

- FG, filament gap, which strongly depends from FD;

- ST, slice thickness, which is the distance (centre to centre) between two adjacent strands on the z-axis;

- LG, layer gap, the height of a single layer, it depends on ST.

Once again, porosity is critic. It depends on filament gap and layers orientation, which can be 0°/90°, 0°/45°/90° and so on, according to the cells to be seeded. Once filament gap is set, if a higher value of RW is chosen, strand distance must change as well, since its value includes filament gap's value and half of the two adjacent strands' RW.

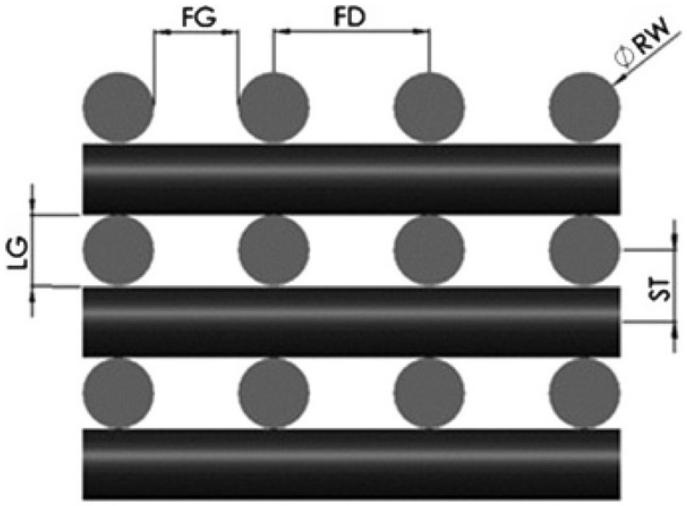

Figure 1.4: Main scaffolds' parameters [5]

1.3 Technologies

During the years different realization methods have been studied and tested. For what concerns scaffold design and realization, technologies can be divided into two macro groups: conventional methods and additive manufacturing methods [1].

1.3.1 Conventional Methods

These are dated technologies, basically manual ones. They provide the realization of a 3D substrate, however they are not able to control pore size and geometry, as well as the spatial distribution of pores (they are not always fully interconnected) [21]. Those parameters are critical to the scaffolds' *in vivo* and mechanical properties [1]. They include methods such as solvent casting / particulate leaching, gas foaming, fiber bonding, phase separation and they usually follow those three steps:

1. a porogen material is put into the discontinuous matrix, so to gain the pores needed to grant cellular adhesion and proliferation;

2. a continuous matrix is formed around those pores;

3. the porogen material is removed.

For example, scaffolds produced by solvent casting/particulate leaching cannot guarantee interconnection of pores because that is dependent on whether the adjacent salt particles are in contact [1].

1.3.2 Additive Manufacturing - AM

As seen in section 1.1.1, additive fabrication processes represent a new group of *non-conventional* fabrication techniques recently introduced in the biomedical field [22]. They allow the realization of well-interconnected, as well as easily reproducible, porous structures, with the help of *3D printing* (3DP). During the last couple of years, 3DP gained a huge success, both in consumer electronics and research. Online communities have born, in which people can share their ideas and their printable files. 3D printers can be used at home, to realize toys, gadgets and utensils, or into a laboratory to do research in different areas of interest, from tissue engineering to aerospatial engineering.

Different 3DP methods exist, according to the type of model realization (material extrusion, powder fusion, photopolymerization, etc.), or to the printed material, that can be thermoplastic or photopolymeric polymers (either natural or synthetic ones), resins, metal powder and so on. A brief list of 3DP methods is shown on Table 1.1. However, all Additive Manufacturing (AM) techniques allow the design and realization of layer-by-layer 3D objects and are characterized by three basic steps in their process: data input, data file preparation and object building [1].

Models to be printed are virtual ones and are designed via CAD (Computer Aided Design) softwares, such as SolidWorks® (*SolidWorks Corp. Boston, MA, USA*). The virtual model (*.stl* file, Solid to Layer) is a series of bi-dimensional cross-sections. It is then processed by a slicer software such as slic3r® (*Ranellucci, A. "Slic3r: G-code generator for 3D printers", 2015*), which creates a mathematical expression of the object, dividing the virtual model into different layers, on te basis of parameters set during slicing process. Basically, the sections are

Technique	Materials	Advantages	Disadvantages
Stereolithography	Reactive resins	Good mechanical strenght, Easy to remove support materials, Easy to achieve small features	Limited to reactive resins (toxic), Limited choice of photopolymerizable and biocompatible liquid polymer materials
Powder Bed Fusion	Ink powder of bulk polymers, ceramics	No inherent toxic components, Fast processing Low costs	Weak bonding between powder particles, Rough surface, Post-processing
Inkjet Printing	Wax, wax compounds	Excellent Accuracy	Slow process, Material limited to low melting point wax
FDM	thermoplastic polymers andceramics	Low costs	Elevated temperatures during process, Small range of bulk materials, Medium accuracy
Selective Laser Sintering	Metals, ceramics, bulk polymers, compounds	High accuracy, Good mechanical strenght, Broad range of bulk materials	Elevated temperatures, Local high energy input, Uncontrolled porosity, Trapped powder difficult to be removed
3D Bioplotting	Hydrogels, thermoplastic polymers, reactive resins, ceramics	Broad range of materials, Broad range od conditions, Incorporation of cells, proteins and fillers	Slow processing, Low accuracy, Limited resolution, No standard condition

Table 1.1: Most popular 3DP techniques [1]

converted into 2D *trajectories* (the *.gcode* file) that the printer's extruder follows, layer-by-layer (the extruder moves along the z-axis) [1].

In biomedical field, fabrication of *customized* devices, which perfectly adapt to the patient's organism and anatomy, could be necessary. For this reason, the CAD model can be created starting from imaging data acquired by Computed Tomography (CT) or Magnetic Resonance Imaging (MRI), which are then *segmented* to extract the region of interest, the object to be printed. This way, AM methods grant the fabrication of objects which are very similar to the originals.

Apart from scaffolds for tissue engineering, 3DP is employed in other medical areas. They can be used to create orthopedic prosthetics at a very low cost, for example to help people from poor countries. Cyborg Beast [23], for instance, is a 3D printed hand for children with traumatic and congenital hand amputations. The hand can be printed at home, by any FDM printer. Its printing and assembling requires no more than 50 USD and a couple of hours. Thanks to this prosthetics, families don't have to worry about the price of the hand that need to be periodically changed, due to child's growth. Moreover, 3DP printed models help surgeons in surgical planning, meaning that they can rehearse a difficult operation, during which they can have low visibility. For example, if they have to operate an aorta, they can

rehearse on that particular aorta's model, thanks to the process seen before.

The two main AM methods in tissue engineering, that will be explained in the next sections are FDM and Bioplotting.

1.4 FDM - Fused Deposition Modelling

FDM uses a moving nozzle to extrude a melted polymeric fiber from which the physical model is built layer-by-layer [1]. The printer can move to the successive layer either moving the extruder or the printbed along the z-axis (Figure 1.5). Support structures can eventually be printed, to sustain overhanging or unconnected parts, then to be manually removed once the printing is done.

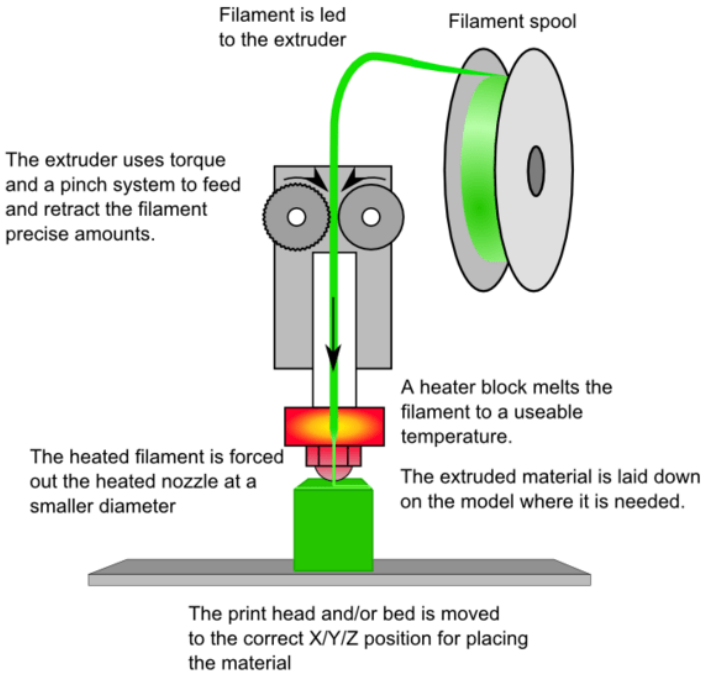

Figure 1.5: Fused Deposition Modelling printing scheme [6]

Printing parameters depend on the extruded material, fabrication conditions, object application field and designer choices. What is really important in tissue engineering is the porosity: it can be achieved modifying the infill density, which defines the amount of plastic used on the inside of the print. All these parameters are set during the slicing process. The most important strand parameters, which can be set in FDM are:

- road width, the diameter of the single extruded strand;
- fill gap, the distance between two adjacent strands' angles;
- slice thickness, the vertical distance (center-to-center) between two strands of two adjacent layers.

While, for what concerns printer's parameters, extruder speed can be set, as well as its temperature, printbed's temperature, and so on. FDM materials are thermoplastic, with good viscous melting properties, such as PLA (Poly-Lactic Acid), PGA (Poly-Glycolic Acid), ABS (Acrylonitrile Butadiene Styrene), and PCL (Polycaprolactone) [1]. Due to the high temperatures, encapsulation of cells and active agents is not possible.

1.5 Bioplotting

3D Bioplotting (or Bioprinting) is a printing technology similar to FDM, as it uses a nozzle to extrude the melted build material into the form of filaments which solidify on the printbed [1]. In 2010 *Guillemot et al* defined Bioprinting as "*the use of computer-aided transfer processes for patterning and assembling living and non-living materials with a prescribed 2D or 3D organization in order to produce bioengineered structures serving in regenerative medicine, pharmacokinetic and basic cell biology studies*" [24].

In our work, *extrusion-based bioprinting* was used. Unlike FDM, where extrusion is driven mechanically by two gears pushing the semi-molten filament, bioplotter's moving nozzle is pressurized, so that the extrusion flow depends on pressure. That is why this type of bioplotters come with an external compressor, which provides compressed air. Some of them also have cross-linking systems, such as UV (ultraviolet) lamps, which stabilize the object once the printing is done.

Bioprintable materials are mostly hydrogels, which do not require high temperature to be extruded, and thermoplastic polymers, such as PCL.

Another important parameter to take into account is the polymer viscosity. The flow rate from the nozzle can be expressed according to the *Hagen-Poiseuille* equation:

$$Q = \frac{\pi \Delta P}{128 l \eta} d^4$$

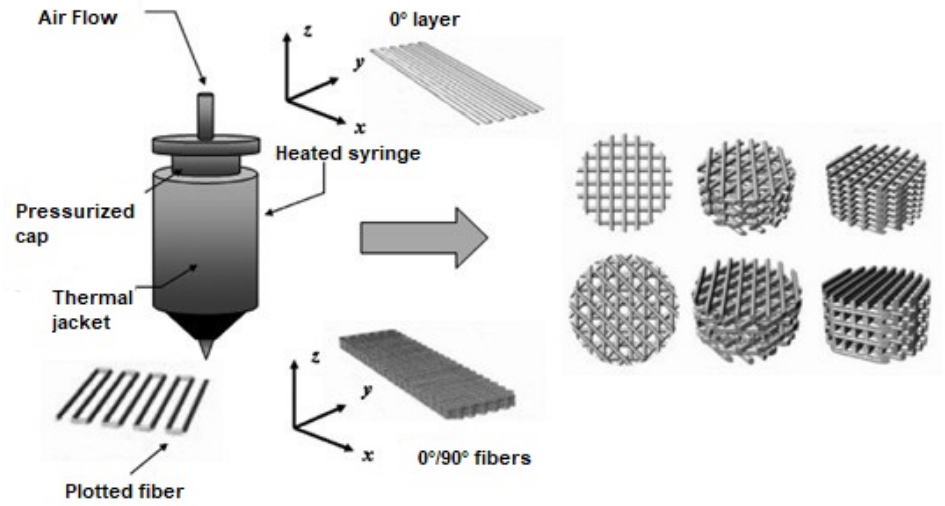

Figure 1.6: Bioplotter's components [1]: on the left, the cartridge where material is loaded and heated, and some printed layers as examples; on the left, scaffolds as printing results

it is directly proportional to the pressure gradient across the syringe and needle tip (ΔP), the needle diameter (d), and inversely proportional to nozzle length (l) and polymer viscosity (η). This means that a high value of Q may result in over-deposition of the fibers, thus reducing porosity, while a low value results in a bad extrusion [1].

Bioplotting's big dream is to print human organs (Figure 1.7), ready to be transplanted. Bioplotter's capacity to extrude living cells incapsulated into a hydrogel (then replaced with cells' ECM), makes this dream less unreal every day. First bioplotting applications dealt with the printing of hydrogels for skin reconstruction. Nowadays scaffolds are printed too, and this technology is becoming essential to tissue engineering.

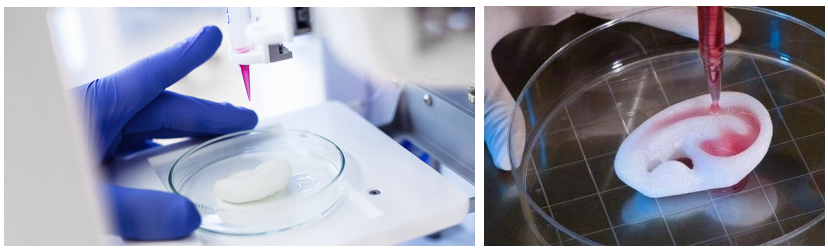

Figure 1.7: Bioplotting applications [7]

1.6 Towards our application: Bone Tissue

All the examined additive manufacturing techniques are widely employed in bone tissue engineering for scaffold realization. That is why in this section, our thesis' ingredients will be shown, starting from the application tissue.

Bone tissue is a connective tissue, different from the others because of its hardness and resistance to pressure, traction and torsion, due to its internal structure, which is crystalline and full of mineral salts. Thus, the tissue can provide stability and sustainment.

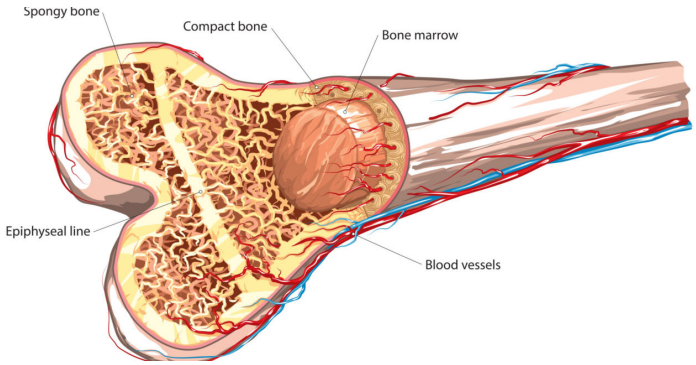

Figure 1.8: Bone's internal structure [8]

It has a really complex hierarchical internal structure: first of all, bone can be structurally distinguished between *spongy* bone and *compact* bone. It is made of inorganic (69%) and organic (22%, the *ECM*) material. The latter gives elasticity and traction resistance, and can be divided into a fibrous part, made for the 90% of collagen fibers, and an interfibrillar part, made of glycoproteins and proteoglycans.

The inorganic matrix gives rigidity and hardness to the tissue. It is made of calcium phosphate, magnesium phosphate, calcium fluoride and needle-shaped *hydroxyapatite* crystals as mineral part. Bones can be long, short or flat.

Another structural partition, which is essential when bone tissue engineering has to be done is between woven and lamellar bone [25].

- **Woven bone**, which is characterised by $5-10\ \mu m$ diameter intertwined collagen fibers. This is the first deposed layer, during both osteogenesis and regeneration.

- **Lamellar bone** which has a regular parallel alignment of collagen into sheets (*lamellae*) and is mechanically strong. Lamellae are organized concentrically around a central canal

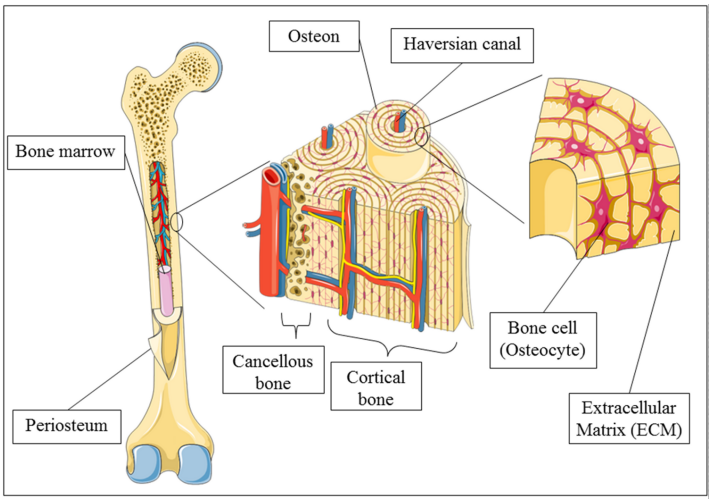

Figure 1.9: Another bone's structural partition [9]

called *haversian canal*. A group of $8 - 10$ lamellae around a canal represent the main lamellar bone unity: the *osteon*, a microscopic column. Osteons tend to merge to create cylinders oriented as the loads the bone has to bear. Each osteon is self-reliant, meaning that its cells take nutrition directly from the vessels inside the haversian canal.

Bone tissue is metabolically active, and composed of several types of cells, such as *osteoblasts*, *osteocytes* and *osteoclasts*, as shown in Figure 1.10.

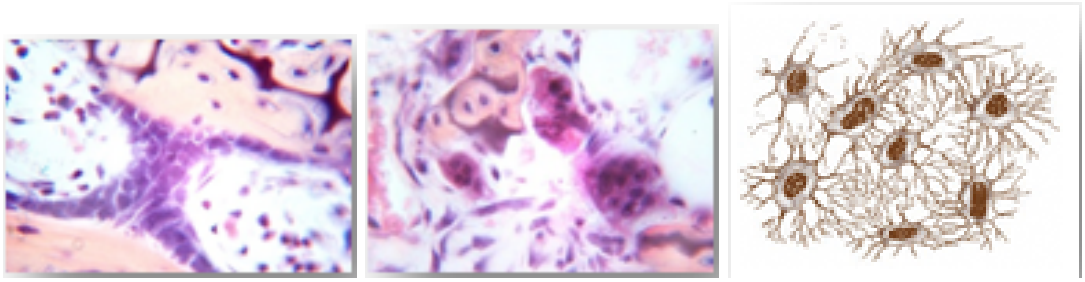

(a) Osteoblasts (b) Osteoclasts (c) Osteocytes

Figure 1.10: Bone tissue cells [10]

Bone tissue has to sustain the entire body, so it shows particular mechanical properties. It is isotropic and viscoelastic (time-dependent behaviour). The mineral phase both increases density and Young's modulus and decreases wreckage work. Plus, humidity plays a crucial role on bones' mechanical behaviour: a dry bone shows a higher elastic modulus and lower wrecking point. Those problems are avoided since its natural environment is wet.

Bone is a smart material, which can adapt to the load it is bearing, optimizing its geometry.

This phenomenon is called *bone reshaping* and follows *Wolff rules*:

1. reshaping is due to bending stresses, not principal ones;
2. reshaping is stimulated by cyclic and dynamic stresses, not static ones;
3. dynamic bending causes a bone growth.

This phenomenon is (maybe) caused by some sort of cells' internal feedback, thanks to which they can feel ECM's deformation state.

All those particular properties have to be taken into account when designing a substitute for this tissue. Bone damages are very common and different one another. In particular, fractures could require several surgical procedures and long recovery periods, as well as the risk of morbidity. The gold standard is the autogenous bone grafting, which may be difficult due to several reasons, such as the shaping process or, in case of other sources, immuno-rejection. Scaffolds and tissue engineering appear to be a good innovation, thanks to the seeding of donor cells on *active*, porous, and biocompatible structures, thus promoting tissue regeneration. Materials and techniques must be chosen knowing that the scaffold will have to sustain loads in particular environments and for particular periods of time [5].

1.7 Biomaterials for bone tissue engineering

1.7.1 Polycaprolactone

Polycaprolactone (*PCL*) is a very common polymer in tissue engineering. Its applications include drug delivvery systems, biodegradable sutures and, of course, scaffolds for bone tissue regeneration. PCL is a semi-crystalline aliphatic polyester. It has the lowest density among polyester plastics. It is prepared by ring opening polymerization of ϵ-caprolactone, using a catalyst such as stannous octoate [26].

What makes PCL unique are its chemical properties. It is highly biodegradable in physiological environment, and this is an essential property for biomedical applications. PCL biodegradation firstly involves ester binding resolution on the main polymer chain, due to external factors, such as organic fluids, and then an intracellular degradation when the polymer's molecular weight decreases [26]. This process is really slow and can be tailored according to the molecular weight and the environment the PCL is put into. Plus, unlike other polyester

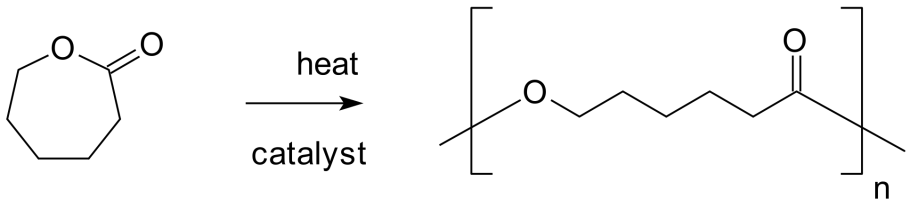

Figure 1.11: PCL synthesis and chemical formula [2]

polymers, its degradation does not produce an acidic environment, providing biocompatibility until the end of its application.

PCL is highly workable, since it is a thermoplastic polymer, with a low melting point of around 60 °C and a glass transition temperature of about −60 °C [26].

However, PCL mechanical properties do not provide the required stability in bone tissue engineering. Thanks to its versatility, it can be mixed with other materials, such as hydroxyapatite, to create a *compound material* with a polymeric matrix (PCL) and an hydroxyapatite reinforcement [12, 27].

1.7.2 Hydroxyapatite

Hydroxyapatite (*HA*) is a calcium phosphate, its chemical formula is $Ca_{10}(PO_4)_6(OH)_2$. It is shown in Figure 1.12.

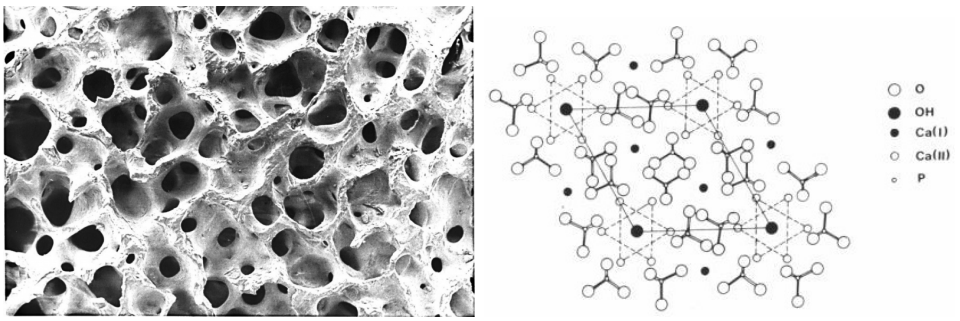

Figure 1.12: Hydroxyapatite [11]

It is a ceramic material, in particular it is the mineral form of calcium apatite. It can be naturally found inside the human body, since it is bone tissue's mineral phase. For this reason it shows a good biocompatibility. Plus, it promotes *osteogenesis*: stem cells tend to differentiate into a bone cell phenotype when in contact with HA (*osteoinduction*), which then helps

osteogenic cells migration into the scaffold (*osteoconduction*), providing its *osteointegration* [28].

All these properties make hydroxyapatite the perfect reinforcement for a bone tissue engineering scaffold made of PCL, which lacks of mechanical properties (as seen in 1.7.1) provided by the HA, in addiction to a higher biocompatibility and bioactivity. Thanks to the presence of HA, bone cells adhesion and functions are stimulated. PCL/HA composites are synthesized dispersing HA powder into a PCL solution, under constant stirring.

1.8 PCL scaffolds for bone tissue engineering: literature review

In bone tissue engineering, PCL has always been the best choice for scaffolds realization. It grants biocompatibility and a slow and tailorable degradation; hydroxyapatite is the perfect reinforcement, since it improves the matrix's mechanical properties and promotes osteogenesis. PCL/HA scaffolds are widely realized, sometimes with some variants.

Reviewing literature on Google Scholar (*https://goo.gl/qKuh3m*) and PubMed (*https://goo.gl/WPV2z5*), using the keywords *'PCL', 'hydroxyapatite', 'scaffold', 'bone'*, a lot of works can be found, and bone tissue engineering history can be traced.

One of the first studies was conducted by *Ciapetti et al.* in 2002 [29]. In this study, micro- and macroporous PCL scaffolds were realized with traditional techniques, phase-inversion and solvent extraction (as seen in 1.3.1). Four PCL-based polymers were realized:

- micro/macroporous PCL;
- HA-added microporous PCL;
- micro/macroporous PCL soaked in Simulated Body Fluid (*SBF)*);
- HA-added microporous PCL soaked in SBF.

Osteoblast-like Saos-2 cells were seeded on the samples, in α-MEM medium. Cells were fed wit complete medium to induce mineral formation. Results showed how viability, measured using the *AlamarBlue* assay, increased in HA-reinforced samples compared to the plain PCL controls, as well as Alkaline phosphatase (ALP), the early marker of mineralization. Cells resulted well spread on the samples' surface and intercellular connections were maintained.

In 2003, *Rohner et al* [30], did not realize reinforced scaffolds, indeed they used bone-marrow to coat them, since it improves bone autograft incorporation. Their work consisted in the study of osteoinductive potential of PCL scaffolds in regenerating orbital defects in pigs, and how this osteoinductivity coul be enhanced by coating. FDM was used to realize those scaffolds. Analysis were conducted on three groups of pigs, according to the defects reconstruction technique:

- no reconstruction (control);
- non-coated PCL scaffolds;
- bone-marrow-coated PCL scaffolds.

All the pigs healed uneventfully. As expected, the control group showed fibrous scar tissue, while the other two groups' defects were correctly reconstructed, and a fibrous tissue layer was found covering the scaffolds, showing how this approach slows regeneration, making it more successful.

Causa et al., in 2006 [31], realized PCL scaffolds reinforced with different volume ratios of HA (13%, 20% and 32%) as well as plain PCL scaffolds as control. Saos-2 osteoblast-like cells were used on 13% and 32% scaffolds, while human bone osteoblasts (HOb) were used on all types of scaffolds. Plain PCL ones showed low mechanical properties. Adding 13% of HA caused hardening of the structure and an increase of both elastic modulus and maximum stress at break. 20% scaffolds showed a decrease in the ultimate tensile strength, while in 32% ones elastic modulus decreased too. The material becomes more brittle. For what concerns biological analysis (in vitro), Saos-2 cells caused ALP release, especially on 13% scaffolds. hOBs' growth was slower on 32% samples. Anyway, adhesion and proliferation values were way higher than the control's.

Park et al., in 2010 [32], used bioplotting to realize plain PCL and PCL/HA (60/40 *w/w*) scaffolds for bone tissue engineering, the latter both with a regular and shifted (SP) printing pattern. Human osteosarcoma MG 63 cells were seeded to study cell adhesion, proliferation and differentiation. Cell proliferation, assessed by MTT assay, resulted in higher values for PCL/HA/SP scaffolds, as for ALP. Reinforced composites showed dense cell layers.

In 2012, *Gloria et al.* [12] doped hydroxyapatite with iron nanoparticles (Fe^{2+} and Fe^{3+} ions), so to gain a FeHA reinforcement with *superparamagnetic* properties, used to realize

PCL/FeHA scaffolds with different w/w ratios (90/10, 80/20 and 70/30), on which human mesenchymal stem cells (*hMSCs*) were seeded. Aside from the usual literature results, magnetic analysis was carried out to assess the magnetization as a function of field and temperature. Magnetic activation enhances bone and vascular remodelling.

Kim et al., in 2013 [33], extracted hydroxyapatite from cuttlefish bone (CB), and realized plain PCL and PCL/HA scaffolds (90/10 w/w) with the solvent casting and particulate leaching technique, using 200/300 μm salt particles as porogens. Human MG-63 pre-osteoblast-like cell were seeded on the scaffolds. In vitro and in vivo experiments were carried out, the latter on rabbits with induced calvaria defects, on which the scaffolds were then implanted. Proliferation resulted higher on reinforced scaffolds. ALP activity increased in cells treated with osteogenic simulator. For what concerns in vivo analysis, neither foreign body reaction nor necrosis was noted. The pore space of the scaffolds was filled with a fibrous connective tissue rich in collagen fibers and fibroblasts.

Ródenas-Rochina et al. [34], in 2013, used hydroxyapatite and *BioGlass* (BG) as reinforcement for PCL scaffolds (5/95, 10/90 and 80/20 w/w). MC3T3-E1, an osteoblast-like cell line, was seeded. Lower BG composition results in higher compressive modulus, while structure weakens as BG increases. However, samples with high concentrations of BG were excluded due to te medium pH drift, which resulted in a phenotypic deviation. Collagen production was surprisingly higher on plain PCL scaffolds. In this study, hydroxyapatite seems to inhibit differentiation: no signs of it were shown up to 28 days.

In 2014, *Gonçalves et al* [35] realized a three-phase scaffold: PCL reinforced with hydroxyapatite and carbon nanotubes (CNT). PCL matrix was 50% of the total, 0-10% of CNT and HA to balance. Scaffolds were soaked in SBF to study bioactivity. MG63 osteoblast-like cells were seeded to analyze spreading. Compressive resistance for low CNT content (0-0.75%), while 10% CNT scaffolds deformed more easily. Bioactivity analysis showed that the samples developed an apatite layer on their surface. Cells adhesion and spreading resulted higher and faster in 10% CNT scaffolds.

Urchin-like and Mg^{2+} -doped hydroxyapatite were used as reinforcement by *Guarino et al.* in 2016 [36], which realized PCL/uHA (urchin-like) and PCL/dHA (doped) scaffolds (13%, 20% and 26% volume ratios), with the solvent casting and particulate leaching technique, then seeded with MG63 human osteoblast-like cells for in vitro tests (cells in empty wells

were considered as control). In vivo tests were carried out on rabbits with induced critical sized defects on te lateral aspect of distal femoral condyles of both paws. Crystal shaped reinforcement resulted in an increase of elastic moudulus, even if for volume ratios higher than 20%, crystal clusters formed and mechanical response drops. Plus, needle-like particles promote the formation of more efficient biomechanical interfaces, as their specific surface is larger. The osteogenic potential of the scaffolds is enhanced too, as well as ALP activity. For what concerns in vivo analysis, no inflammation phenomena was observed until 12 weeks. Regeneration started from the periphery towards the center of the scaffolds. There were no big differences between uHA and dHA samples, except for a higher quantity of trabecular bone in dHA regeneration.

Zheng et al., in 2017 [27], immersed the PCL/HA scaffolds (60/40 w/w), realized via FDM, in unprocessed bone marrow blood (UBMB) taken from rabbits, so to create a coating and the formation of marrow clots (MC). This was carried out in two ways, according to the MC formation procedure:

- Group A (MC enriched): scaffolds were immersed in rabbit's UBMB;
- Group B (MC combined): scaffolds were plugged into the rabbit's micro-fracture.

Mesenchymal stem cells were seeded on the coated scaffolds. ALP activity increased with time, and resulted greater in group B. Osteogenic differentiation and adhesion were higher in both groups.

All those studies are summarized in Table 1.2, where the outcome consists in the improvements the reinforcement brings to the scaffold.

One thing that can be noticed is that reinforcement ratio is never higher than 40%. That is because it was proved that mechanical properties gets better as the reinforcement increases. However beyond a specific limit of hydroxyapatite amount, by further increasing the concentration, the mechanical performances of the nanocomposite substrates decrease because the HA's nanoparticles act as 'weak points' instead of reinforcement for the polymeric matrix [12].

1.9 Thesis Goals

This thesis main goal was to print PCL/HA scaffolds for bone tissue engineering, in 90/10 polymer-to-reinforcement weight ratio (w/w). 80 kDa plain PCL was used as control. The

Author and Year	Reinforcement (w/w)	Fabrication Technique	Cells seeding	In vivo / in vitro Tests	Outcome
Ciapetti et al. (2003)	40% HA	Phase-inversion Solvent extraction	Saos-2	In vitro	Higher viability Better ALP release Increased calcium deposition
Rohner et al. (2003)	//	FDM	Bone-marrow coating	In vivo - pigs with orbital defects	All pigs healed uneventfully Higher bone remodelling
Causa et al. (2005)	40% HA 70% HA 132% HA	//	Saos-2 Human bone osteoblasts	In vitro	Higher migration Cells reach confluence and keep differentiation
Park et al. (2010)	40% HA	Bioplotting	Human osteosarcoma MG 63 cells	In vitro	ALP activity increased Better mechanical properties Better adhesion and proliferation
Gloria et al. (2013)	10% HA 20% HA 30% HA HA iron-doped	FDM	Human mesenchymal stem cells	In vitro	Magnetic activation - helps bone remodelling Better mechanical properties Better adhesion, proliferation and differentiation
Kim et al. (2013)	10% HA	Solvent casting Particulate leaching	MG-63 pre-osteoblast-like cells	In vitro In vivo - rabbits with calvarial defects	Cell proliferation increased Better adhesion
Ródenas-Rochina et al. (2013)	5, 10, 20% HA and Bioglass	Particle leaching Freeze extraction	MC3T3-E1	In vitro	Compressive modulus/elastic limit increases for low HA/BG concentrations Higher seeding efficiency
Gonçalves et al. (2015)	0 - 10 % CNT (Carbon nanotubes) 40 - 50 % HA	Bioplotting	MG-63 osteoblast-like cells	In vitro	Higher bioactivity and adhesion in the scaffolds with 10% CNT
Guarino et al. (2016)	13%, 20%, 26 % (v/v) uHA (urchin-like) dHA (MG^{2+}-doped) 10% chloride crystals	Solvent casting Particulate leaching	MG-63 osteoblast-like cells	In vitro In vivo - rabbits with distal femoral condyles defects	Mechanical response increased Higher ALP activity Higher proliferation No inflammation phenomena Good regeneration
Zheng et al. (2017)	40% HA	FDM	Mesenchymal stem cells Scaffolds immersed in UBMB	In vivo - rabbits with condyle and distal femure fractures	Better adhesion and proliferation Improved osteogenic differentiation

Table 1.2: Bone tissue engineering literature overview

aim was to show how HA reinforcement enhances both mechanical and biological properties. These scaffolds have to satisfy several requirements:

- strand diameter: 300 μm;
- filament gap: 300 μm, which automatically defines a strand distance of 600μm;
- slice thickness: 300μm for plain PCL scaffolds and 240 μm for reinforced ones;
- layers orientation: 0°/90°.

In particular, scaffolds are cylinders with a 6 mm diameter. Half of them are 2 mm high, the other half 6 mm high. The former were used for biological analysis, the latter for mechanical analysis.

The first step of the work has been to characterize plain PCL bioprinting, using a commercial pneumatic-based bioplotter, analyzing different pressure/speed combinations for different nozzle diameters, starting from literature parameters, since it is quite rare to find articles which specify printing parameters for bioplotters.

This thesis follows literature trends (it is close to the works made by *Gloria* in 2013 and by *Park* in 2011), analyzing how reinforcement improves the scaffolds' behaviour, both

mechanical and biological. This is why, after the scaffolds were printed, compression tests were carried out, then *Human Mesenchymal Stem Cells* (hMSCs) were seeded on them, and their viability measured.

This work was conducted in collaboration between the Computational Mechanics and Advanced Group (Comp-Mech, DICAr, UniPV) where PCL characterization was carried out and scaffolds were printed, and in Naples, at the *Istituto per i Polimeri Compositi e Biomateriali - Consiglio Nazionale delle Ricerche* (IPCB-CNR), where compression and cells viability tests were conducted.

Chapter 2

3D Printer set-up

In this chapter, the PCL/HA compound material synthesis will be shown, and then the used commercial 3D bioplotter (Cellink INKREDIBLE+) will be presented. Finally, the PCL characterization procedure will be discussed, and its results will be shown in the end.

2.1 PCL/HA compound pellets

PCL/HA compound material was synthesized embedding HA into a PCL matrix.

- *Day 1*: firstly, 15 grams of PCL pellets (M_w = 80000 Da, *Sigma-Aldrich, BVBA, Diegem, Belgium*) were dissolved in tetrahydrofuran (THF) under hood at room temperature [12], using a magnetic stirrer and a little magnet inside the beaker. The proportion is: 80% of solvent and 20% of PCL. That is why 60 grams of THF were added.

- *Day 2*: hydroxyapatite powder (*Sigma-Aldrich, BVBA, Diegem, Belgium*) was added, in particular 1.67 grams. Each particle is 30 nm big.

- *Day 3*: the stirring compound was put into an ultrasonic bath (Branson 1510 MT) to optimize the reinforcement dispersion in the polymer solution, so not to have repeatability issues when printing. The compound was then poured into a beaker filled with ethanol to obtain solvent extraction. The resulting PCL/HA "*dough*" was then spread onto an aluminium foil, and left drying for 24 hours under hood. That way, remaining THF traces evaporated.

- *Day 4*: the dry compound was manually cut into small pellets. Dimension homogeneity is not necessary, since those pellets were to be melted into the bioprinter's cartridge.

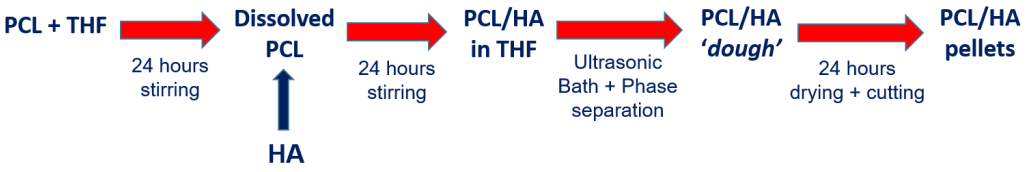

Figure 2.1: PCL/HA synthesis scheme

(a) PCL dissolved in THF

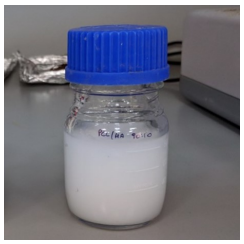

(b) PCL/HA solution in THF

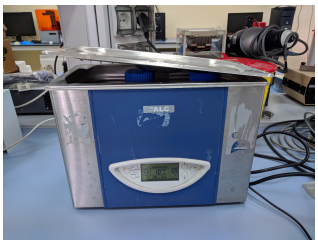

(c) Ultrasonic Bath

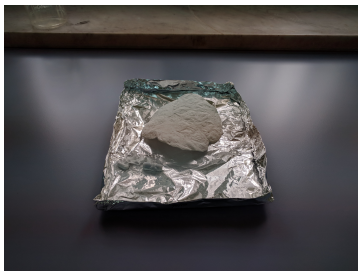

(d) The dry compound

(e) Plain PCL and 90/10 pellets

Figure 2.2: PCL/HA synthesis, from PCL dissolution (a) to pellets cutting (e)

2.2 TGA - Thermogravimetric Analysis

A thermogravimetric analysis under air was carried out to thermally characterize our pellets. Quantity measured was pellets' weight loss ratio (degradation) under high temperatures, since they had to be melted inside the bioprinter's cartridge. A TGA Q5000 (*TA Instruments, LTD*) thermogravimetric scale was used to carry out this test.

Samples were heated up to 700°C with a speed of 10°C/min, allowing us to estimate sample's weight loss ratio as temperature varies. Our goal was to find a *limit temperature*,

that corresponds to the beginning of the PCL matrix degradation, which ends with only the inorganic phase (HA) left on the scale; there is also a second limit temperature, which is the mineral phase degradation one.

This analysis was conducted to make sure that chosen printing temperature (120 were not to compromise our pellets.

2.2.1 Results

TGA was conducted on the PCL/HA pellets to analyze their thermic degradation behaviour.

Samples were subjected to a thermic degradation process starting from $230 \pm 10°C$, that is the temperature at which the PCL matrix started degrading. This process leads to a complete matrix degradation at around $400 \pm 10°C$. At this temperature, only 11% of the material was found as residual, which analyzing our PCL/HA 90/10 (w/w) pellets, corresponds to the hydroxyapatite nanoparticles (10%). To find their degradation temperature, higher temperatures have to be investigated.

2.3 Cellink INKREDIBLE+

The 3D bioplotter used to print PCL is the INKREDIBLE+, made by *Cellink* (*Cellink AB, Sweden*). It is located in the Experimental Surgery Laboratory at the University of Pavia, providing ideal environment to guarantee samples sterility.

It is a pneumatic-based bioplotter, with a chamber cleaning system and a UV lamp. There are two heated extruders, which move along the x-y axes, while the printbed moves along the z axis. INKREDIBLE+ comes with an external air compressor, which provides air flow. INKREDIBLE+ allows to extrude hydrogels (viscosity range from 0.001 to $250 Pa * s$). It comes with nozzles of different sizes, depending on user's needs. The bioplotter allows to print PCL pellets too, thanks to specific aluminium cartridge and nozzles, which resist to the high temperatures the pellets need to melt.

Main printer's parameters are shown in Table 2.1.

INKREDIBLE+ can print different kind of cells, such as *mesenchymal stem cells*, *chondrocytes*, *fibroblasts*, *iPSC-derived cardiomyocytes*, *osteoblasts*, *myoblasts*.

Extrusion system	Pneumatic-based
Print-heads	2 heated print-heads
Air Supply	External Compressor
Build Volume	130 x 80 x 100 mm
File Input	SD card and USB connectivity
UV Crosslinking system	365 nm, 405 nm wave lengths
XYZ resolution	10 μm
Air Filter	HEPA H13
Maximum operating pressure	700 kPa
Set Pressure Range	5 to 400 kPa
Layer Resolution	100 μm

Table 2.1: INKREDIBLE+ main features

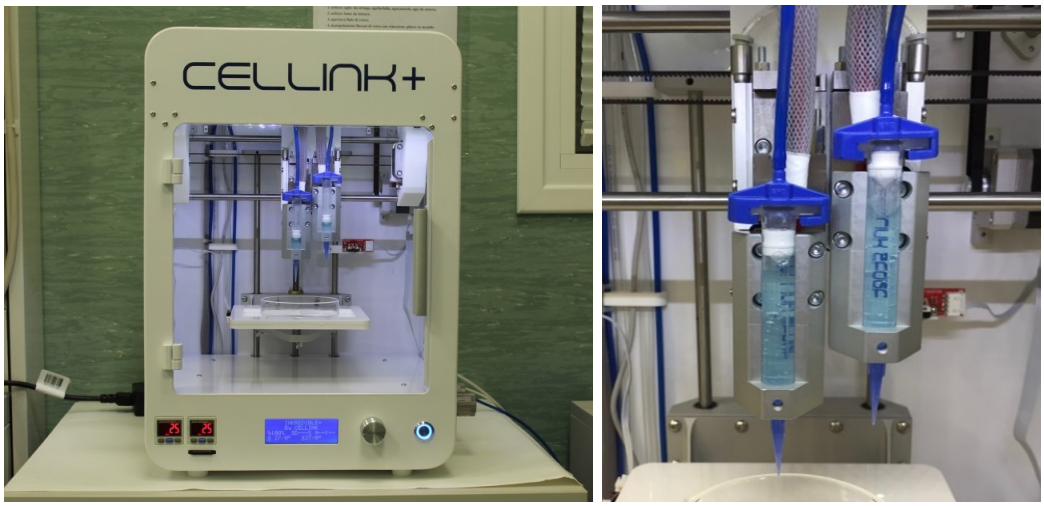

Figure 2.3: Cellink INKREDIBLE+

2.4 Printing Parameters

In order to characterize PCL, a literature research was done. The acquired printing parameters were then the starting point to a range defining for PCL characterization. Most of the studies refer to a plain PCL bioprinting.

In 2017, *Neufurth et al.* [4] bioprinted PCL/CA^{2+} scaffolds, as well as plain PCL ones as control, for bone regeneration. They showed how those scaffolds matched cortical and trabecular bone's mechanical properties with morphogenetic activity. Plus, they were capable of attracting and promoting the growth of human bone-related cells.

Bartolo et al. [37] analyzed a new bioprinter prototype, the *BioCell Printing*, which

Parameters	*Neufurth et al.*	*Sheshadri*	*Bartolo et al.*	*Cellink*	*Lab Experience*
Pressure [bar]	8	[3.5 - 5]	5	[1.10 - 1.40]	8
Temperature [°C]	100	[70 - 100]	80	100	120
Strand diameter [μm]	300	circa 500	300	//	300
Strand distance [mm]	1.4	1/1.75	0.650	//	0.6
Nozzle size [mm]	0.3	(0.2, 0.3, 0.4)	0.3	0.7	0.3
Extrusion speed [mm/min]	180	[60 - 90]	420	[30 - 270]	30
Layer thickness [mm]	0.3	0.3	0.28	//	80% of diameter
Layers orientation	0 - 45°	0 - 90°	0 - 45°		0 - 90°

Table 2.2: PCL bioprinting parameters in literature

provides the integration of all bioprinting stages (matrix printing, sterilisation and seeding) in a fully automated bench-top manufacturing system. PCL was selected to test that machine.

Priyanka Sheshadri, in her PhD thesis [38] actually characterized PCL (M_w = 43000/50000 Da) bioprinting, for different nozzle sizes, temperatures and pressures, as well as printing speed. However, she used a different machine: her parameters have been essentials as a starting point.

Via private communication, Cellink sent some PCL printing parameters, the ones used for their INKREDIBLE+ characterization, which was a more generic one: they were interested in minimum printing conditions, in fact they used low pressures and high nozzle diameters.

Based on his experimental experience in the field, professor *Antonio Gloria*, from the Naples' *IPCB-CNR*, where biologic analysis on the scaffolds were conducted, suggested other parameters.

All the acquired printing parameters are shown in Table 2.2, where also scaffold ones are present. Starting from literature, a testing range for INKREDIBLE's PCL characterization was set, as shown in Table 2.3.

Pressure	(4.5 - 5.0 - 5.5) bar
Temperature	130°C
Extrusion Speed	(30 - 60 - 90) mm/min
Nozzle size	(0.3 - 0.5 - 0.7) mm

Table 2.3: Characterization parameters

2.5 PCL Characterization

The goal of this process is to understand which strand thickness given pressure/extrusion speed values realize. In order to get the desired strand diameter, 300 μm, once the nozzle is set, the right pressure/speed combination has to be found. In general, if pressure is set, high speeds create thinner strands, while low ones thicker strands. When using small nozzle diameters, polymer viscosity can be reduced adding specific solvents, however putting biocompatibility at risk [1].

First, we characterized Cellink-provided PCL (M_w=50 kDa, 3 mm pellets) and then the "home-made" plain PCL (M_w=80kDa) and PCL/HA 90/10 (w/w) pellets.

2.5.1 Bioplotter set-up

Printer set-up consists on the following steps:

1. the printer's cartridge is filled;
2. temperature is set to 120°C;
3. PCL is left to melt for 30 minutes (after the temperature is reached);
4. home axes: it is an automatic process, with which the printer sets the extruder (x-y axes) and the printbed (z axis) on their zero, thanks to limit switches. That is an essential step to do when starting a new print;
5. z-axis calibration, manually, to the set layer height;
6. printhead is opened and some material is extruded, so to load the nozzle.

2.5.2 Characterization protocol

For each nozzle size (0.3 mm, 0.5 mm, 0.7 mm), tests were conducted at a set pressure: three strips of PCL were extruded, one for each extrusion speed value (30 mm/min, 60 mm/min, 90 mm/min); then, pressure was raised. In Figure 2.4 there are all the possible values combinations: points on the same row represent a single test.

Each test was conducted three times: this means 9 tests for each nozzle. The three strips were extruded on a glass *Petri dish*, then photographed (Canon EOS 1200D): camera zoom was set to x36 and its distance from the photography surface was 13 cm.

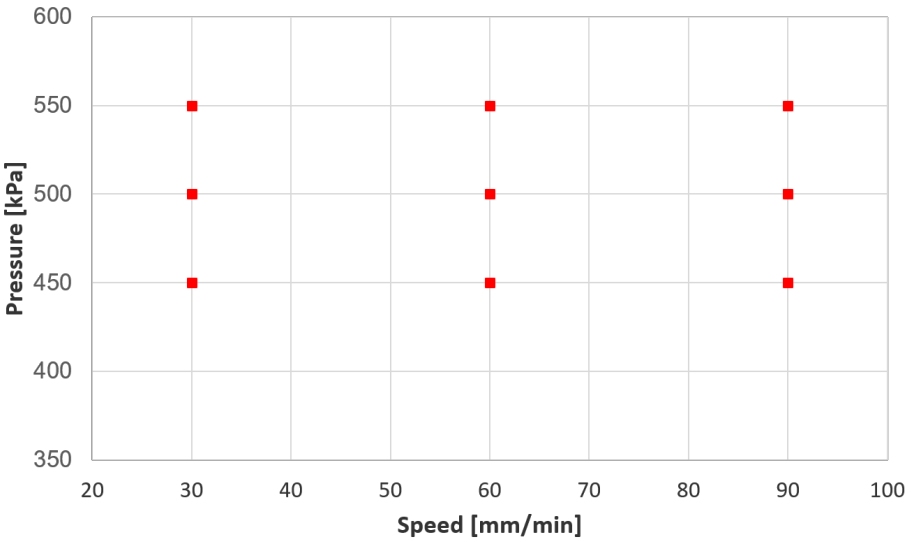

Figure 2.4: Speed/Pressure combinations

Set printing parameters were:

- printer's temperature: 120°C;
- nozzle's height from extrusion plate: 300 μm, since the aimed layer's height is 0.3 mm;

2.5.3 Strands analysis

Each test's Petri was photographed (as shown in Figure 2.5(c)) and then the thickness measured.

For this work, a semi-automatic process was applied. To do so, first the image had to be pre-processed via an imaging software, FIJI® ("Fiji Is Just ImageJ", *Rasband, W.S., ImageJ, U. S. National Institutes of Health, Bethesda, Maryland, USA,* http://rsb.info.nih.gov/ij/). *Magic Wand* tool was used to create, manually, a segmented mask of the image, as shown in Figure 2.5(d). Although this is a manual process, it is more precise, since the tool automatically gathers pixels with a similar grey level. So, if the PCL stripe is brighter than the background, segmentation is more effective. A piece of graph paper was used as landmark (Figure 2.5(a)) and pre-processed.

Once the image was pre-processed, a script was realized on MATLAB® R2017b (*MathWorks, Inc., Natick, MA, USA*). The number of strands to analyze and both nozzle diameter and pressure are selected by user. According to those choices, the script uploads the three

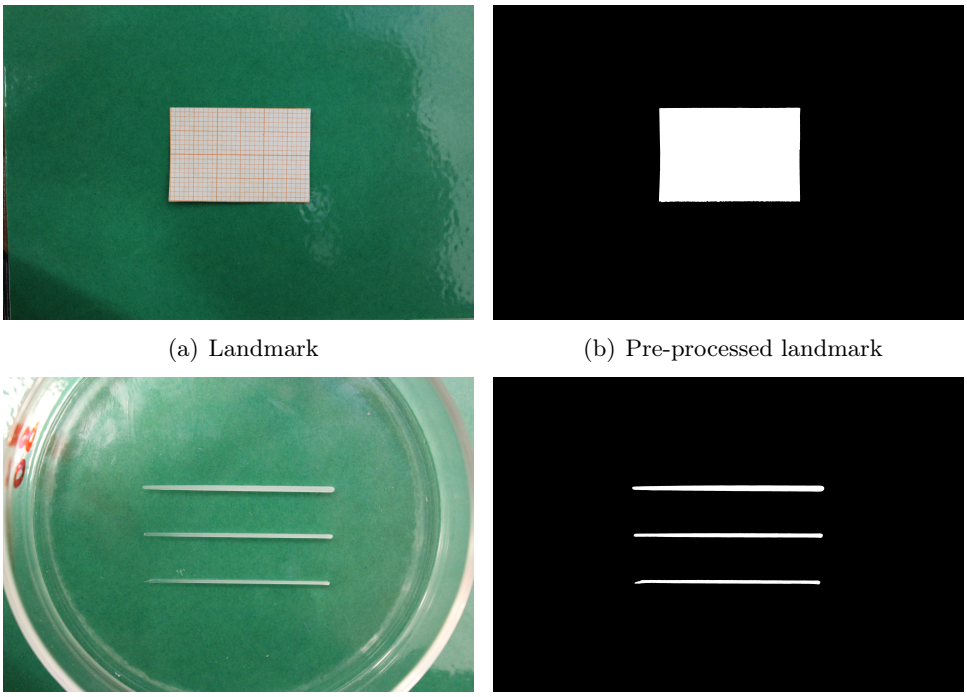

(a) Landmark (b) Pre-processed landmark

(c) Original photo (d) Pre-processed image

Figure 2.5: Tests on Cellink's PCL

tests' images and binarizes them. User then has to crop the photo to select the strands to measure. The landmark has to be cropped too. At this point, each strand is a cell-array, made of the three tests' strands. Thickness, in pixels, is evaluated for each column, which is a vector, as the difference between the last and the first white cell's index. The same process is applied to the landmark, whose length in pixels is needed to find thickness in millimeters.

Even if pre-processing and binarization are quite precise, there is a noise removal function, which deletes possible external white dots that could invalidate the measurement. This function is triggered when two consecutive white cells' indexes are not consecutive numbers.

Once thickness in pixels and millimeters is evaluated for the whole strand length, mean value and standard deviation are calculated.

2.5.4 Results

Characterization results are shown in Table 2.4.

Results for the 0.3 mm nozzle at 90 mm/min are not shown, because the chosen pressures were not high enough to allow PCL extrusion at that speed: of course, the higher is the nozzle

		Strand diameter [mm]		
		30 mm/min	60 mm/min	90 mm/min
0.3 mm	450 kPa	0.32 ± 0.03	0.30 ± 0.04	//
	500 kPa	0.34 ± 0.03	0.30 ± 0.04	//
	550 kPa	0.38 ± 0.03	0.32 ± 0.06	//
0.5 mm	450 kPa	1.06 ± 0.13	0.75 ± 0.07	0.67 ± 0.08
	500 kPa	1.15 ± 0.17	0.82 ± 0.09	0.70 ± 0.07
	550 kPa	1.27 ± 0.21	0.91 ± 0.10	0.76 ± 0.06
0.7 mm	450 kPa	1.64 ± 0.12	1.05 ± 0.08	0.83 ± 0.07
	500 kPa	1.78 ± 0.17	1.19 ± 0.11	0.93 ± 0.10
	550 kPa	1.90 ± 0.15	1.29 ± 0.10	1.05 ± 0.11

Table 2.4: PCL characterization results

diameter, the lower is the minimum pressure required to extrude. In addition to this table, graphic results for each extrusion speed are shown in Figure 2.6.

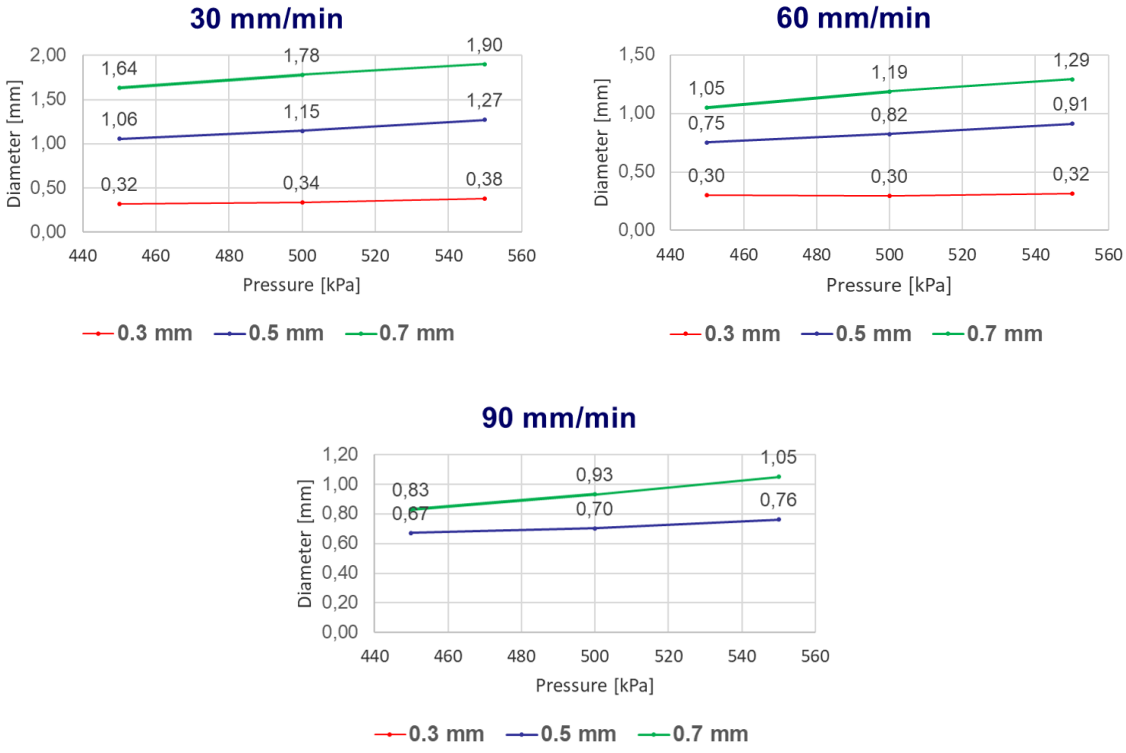

Figure 2.6: Characterization results for each extrusion speed

Increasing nozzle size increases strand thickness, as well as increasing extrusion speed decreases it.

Reminding our strand size target, which is a $300\mu m$ strand diameter, for which a layer

height of 0.3 mm was set, it is clear that the 0.3 mm nozzle grants the best diameter values, as expected.

Another interesting point of view consists in analyzing these results for each nozzle, as shown in Figure 2.7.

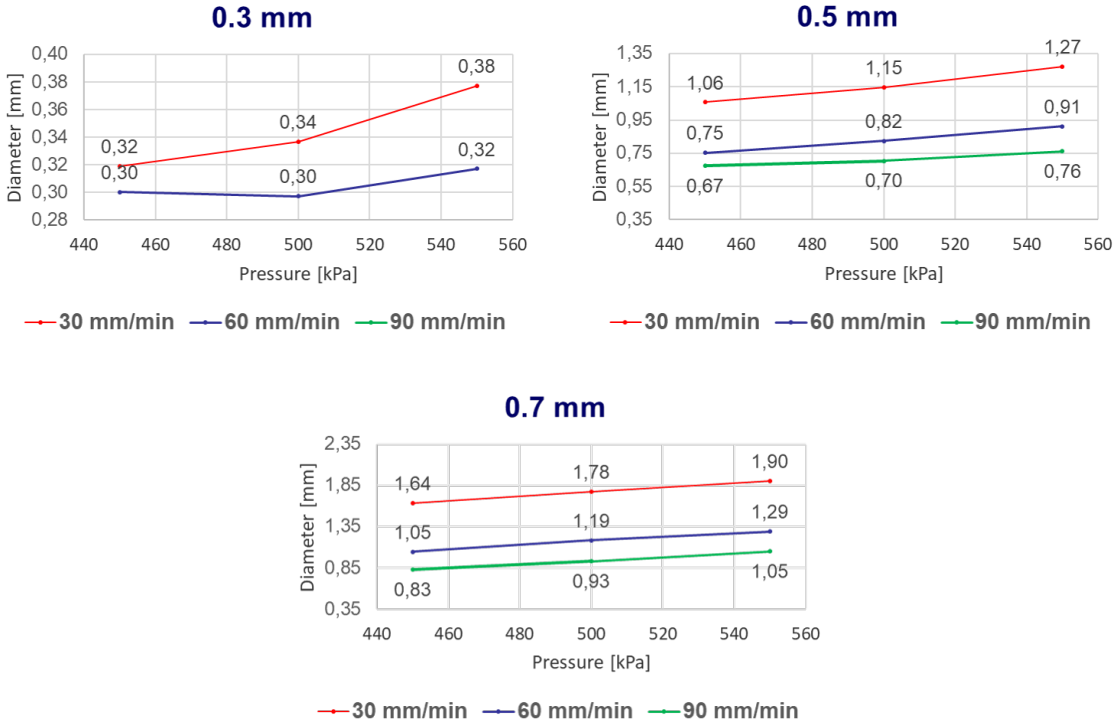

Figure 2.7: Characterization results for each nozzle

For a given nozzle size, strand thickness increases with printing pressure and this result is confirmed for any of the considered extrusion speeds. As expected, since layer height was set to 0.3 mm, strands extruded from the 0.5 mm and 0.7 mm nozzles resulted spreader, and thus the word 'thickness' seems more appropriate than 'diameter'. In the 0.3 mm diagram, the blue curve related to the 60 mm/min extrusion speed initially slightly decreases, then increases like all the other curves. This means that apparently strand diameter decreases as pressure increases. This was not considered as a mistake: the two diameters, taken with all the decimal places, are 0.30039 mm for 450 kPa and 0.29783 mm for 500 kPa. This means that the second strand is 2.54 μm thinner. This difference is minimal, and so the two diameters are both rounded to 0.3 mm.

2.5.4.1 80 kDa PCL

Once those results were obtained, assuming a similar behaviour for both 50 kDa and 80 kDa PCLs, repeatability tests were carried out with particular pressure/speed couples, which are all the considered ones for the 0.3 mm nozzle, except for the 550 kPa - 30 mm/min. Results were similar, as shown in Table 2.5 and Figure 2.8.

	30 mm/min	60 mm/min
450 kPa	0.33 ± 0.025	0.27 ± 0.048
500 kPa	0.35 ± 0.026	0.29 ± 0.028
550 kPa	//	0.28 ± 0.016

Table 2.5: 80 kDa PCL characterization

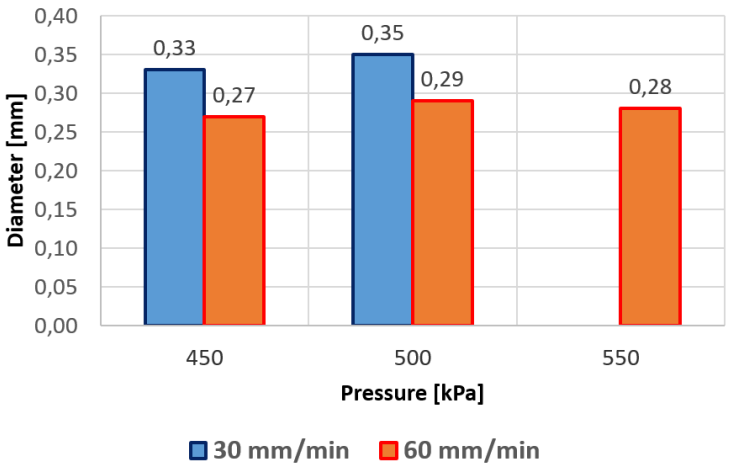

Figure 2.8: Strand diameter evaluation for 80 kDa PCL

It is easy to see that for the 60 mm/min extrusion speed, strand diameter seems to decrease when pressure increases from 500 kPa to 550 kPa. This is not true: as it can be seen, the latter standard deviation is smaller than the former, thus the 500 kPa strand can be 0.028 mm thicker or thinner.

Once it was proved the two PCLs' behaviour is similar, since 80 kDa PCL was to be used to print scaffolds as well, strand distance measurements tests were conducted on a single scaffold layer, as shown in Figure 2.9. Its design will be discussed in paragraph 3.1. Strand distance measurements were similar to the strand diameter ones, pre-processing the images via FIJI and analyzing them with MATLAB.

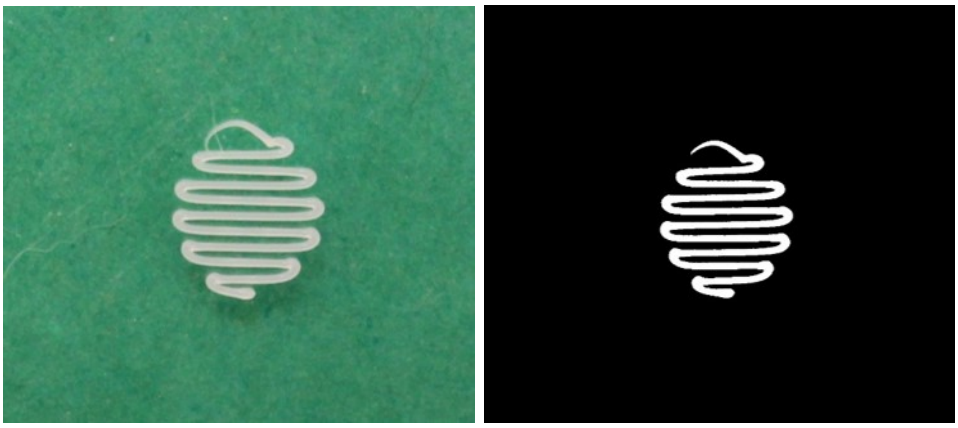

Figure 2.9: Scaffold's single layer

An extrusion speed of 45 mm/min was analyzed too, so to better investigate the values interval.

Single layers' strand distances results for 80 kDa plain PCL are shown on Table 2.6 and Figure as mean values.

	Mean Strand Distance
450 kPa - 45 mm/min	0.2863
500 kPa - 45 mm/min	0.2573
500 kPa - 60 mm/min	0.2879

Table 2.6: Strand distance values on single scaffold's layers

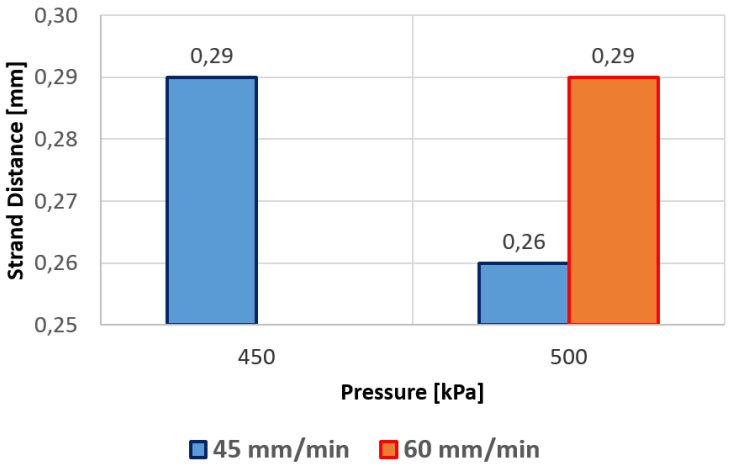

Figure 2.10: Strand distance evaluation for 80 kDa PCL

First tests were conducted for a 500 kPa pressure: once it was clear that higher pressures

resulted in smaller strand distances, ranges were modified. That is why only three couples of values were analyzed.

Even if 500 kPa - 60 mm/min and 450 kPa - 45 mm/min resulted in similar strand distance values, the latter couple was chosen to print plain PCL scaffolds, since a lower speed was preferred.

2.5.4.2 Reinforced PCL

Similar tests to the ones seen in paragraph 2.5.4.1 were conducted on PCL reinforced with 10% HA (Figure 2.11.

As expected, minimum extrusion pressure was higher than the plain PCL one. In particular, for our PCL/HA 90/10 scaffolds, pressure was set to 650 kPa, and extrusion speed to 45 mm/min, which provided a mean value of strand distance of 0.3059 mm.

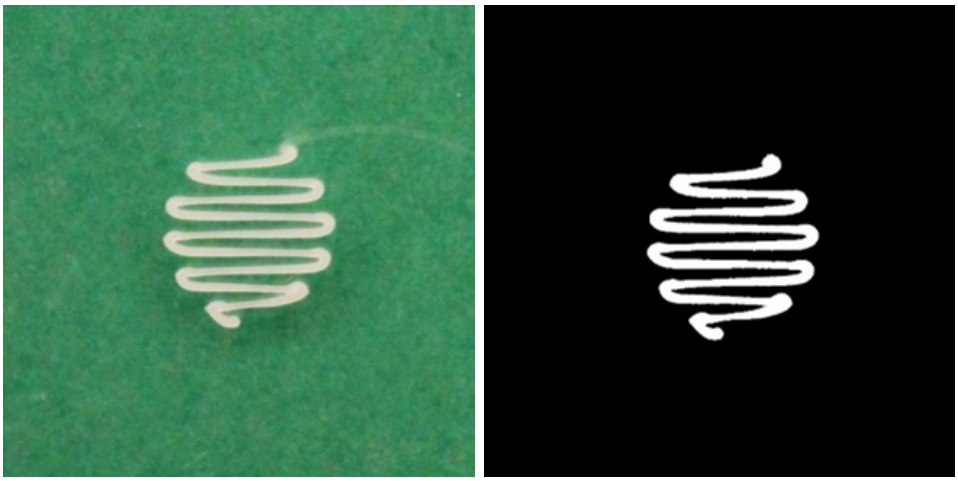

Figure 2.11: Strand Distance analysis on a scaffold's single layer for PCL/HA 90/10 (w/w)

Chapter 3

Scaffolds Manufacturing and Analysis

This chapter deals with the thesis core, which is the scaffolds fabrication and analysis. First, the scaffolds were designed and printed. After that, they were brought to Naples to characterize their mechanical behaviour with compression tests. Human Mesenchymal Stem cells (hMSCs) were seeded on half of the scaffolds, and their viability measured with the Alamar Blue Assay.

3.1 Scaffold design

The scaffold was designed using a CAD software, SolidWorks.

First of all, a 2D sketch was drawn. The aim was to reproduce the nozzle path on the printbed: that is why a 6 mm diameter circle was sketched as a guide, since a cylinder had to be drawn. Several vertical guidelines were traced, 0.6 mm distant from each other (the dotted lines in Figure 3.1(a)). To get the strand, two vertical lines for each guideline were drawn: one of them 0.15 mm distant on the left of the guideline, the other one on the right. All the vertical strands were then connected one another, and so a single scaffold layer was done.

Once the single layer was done, the two scaffold types could be made as an *assembly* of it. A first layer was secured on the plain and copied: this second layer was then moved for 0.3 mm along the z-axis and rotated 90°. This process was repeated until the desired geometries were obtained: 7 layers for the 2 mm high cylinder (2.10 mm, actually), and 20 layers for the 6 mm high one, as shown in Figure 3.1(c) and Figure 3.1(d).

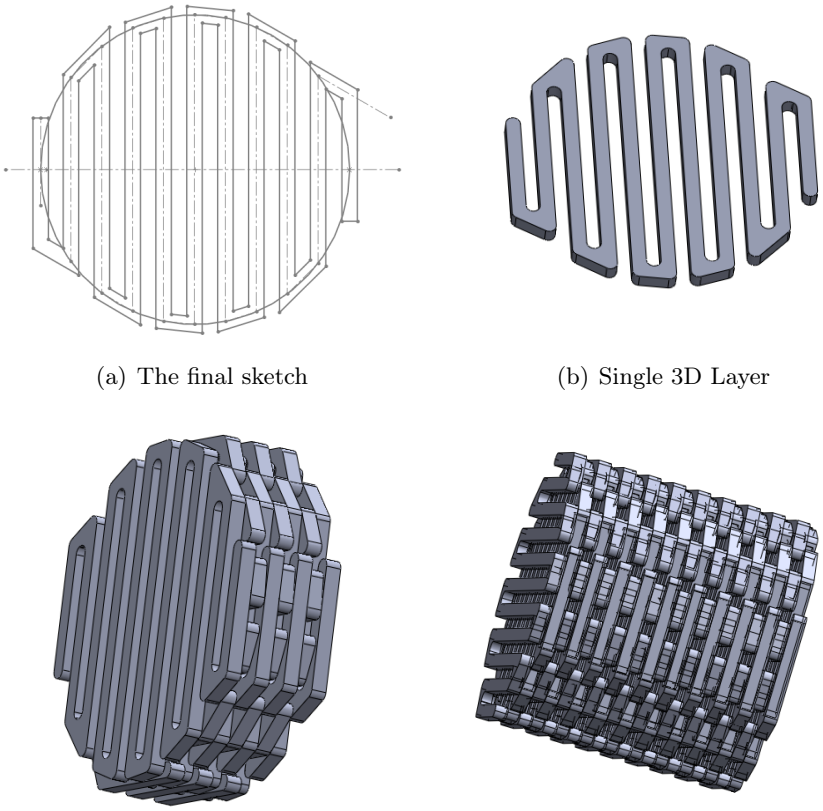

(a) The final sketch

(b) Single 3D Layer

(c) 2 mm high scaffold

(d) 6 mm high scaffold

Figure 3.1: Scaffolds design

3.1.1 Slicing process

Once the stl file was done, it was loaded into a slicing software, Slic3r.

As already said in paragraph 1.3.2, the slicer returns a series of coordinates, the *.gcode* file, which turns into 2D trajectories the printhead has to follow.

Cellink provided a suggested set of slicing parameters, including printbed dimensions, as well as a post-processing script, which is run by the slicer, since some common slicing parameters, such as strand thickness, printhead temperature (which is set manually on the printer) and flow rate are not to be taken into account for a bioplotting process, where pressure and speed are the main parameters.

A list of printing parameters set on slic3r for each type of material is shown in Table 3.1.

	Plain PCL	**PCL/HA 90/10**
Pressure [kPa]	450	650
Temperature [°C]	120	120
Extrusion speed [mm/min]	45	45
Layer heigth [mm]	0.3	0.24

Table 3.1: Scaffolds printing parameters

3.1.2 Layer height

It is easy to notice that in Table 3.1, two different layer heights (measured as center-to-center distance between two adjacent strands on the z axis) are shown, one for the plain PCL scaffolds and one for the HA reinforced ones. A layer height of 0.3 mm for the plain PCL scaffolds was chosen reviewing literature [4, 38]. This way, some stability issues could arise: ideally, if strand diameter is 0.3 mm as well as layer height, there is only one tangency point between the two adjacent strands. This could cause structure collapse. In spite of that, those problems did not show while printing plain PCL scaffolds.

However, when starting printing reinforced PCL, structures collapsed. Both literature [37] and professor Gloria's parameters suggest that, when printing a composite material, layer height, should be circa 80% of strand diameter.

That is why, for our PCL/HA 90/10 scaffolds, layer height was set to 0.24 mm.

3.2 Printing Process

At this point, scaffolds were ready to be printed. As previously said, layers pattern was set to 0°/90°.

For both plain PCL and PCL/HA 90/10, eight 6 mm high and fifteen 2 mm high scaffolds were printed. The former for mechanical analysis, and the latter for biological ones. Samples number is due to statistic ends.

In Figure 3.2 the two types of printed scaffolds are shown.

3.2.1 Limitations and possible solutions

The Cellink INKREDIBLE+ is a commercial entry level bioplotter. So, it comes with some limitations, which can be crucial when printing PCL. One of those surely is the maximum working pressure, which is 700 kPa. Actually, when it is higher than 550 kPa, the printer's

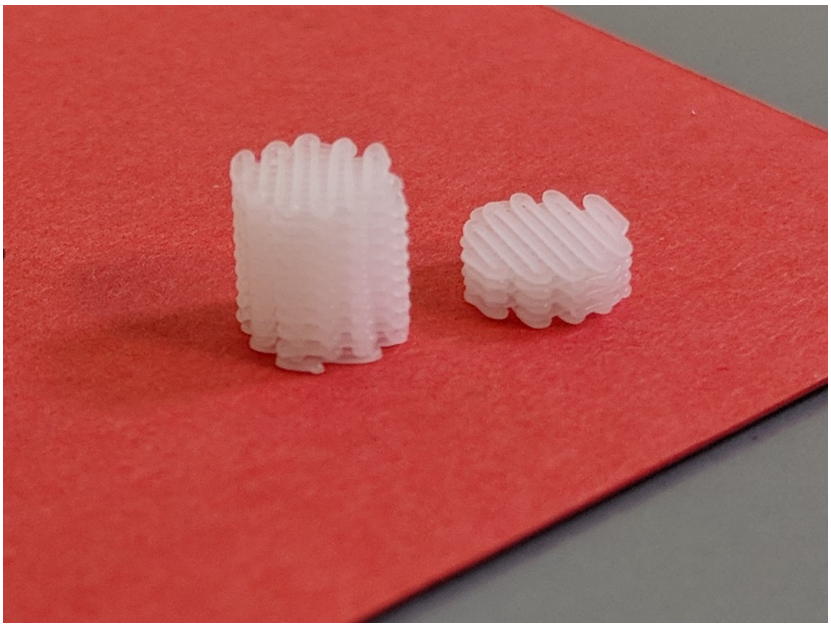

Figure 3.2: 6 mm and 2 mm high printed scaffolds

sensor stops working, and everything has to be checked and set directly from the pressure line. Those problems prevented us from printing compound materials with higher reinforcement percentages, such as PCL/HA 80/20, which is quite common to find in literature. Other than that, we found INKREDIBLE+'s nozzles, which are provided by Cellink itself, quite brittle, they pretty easily broke on the tip. Furthermore, the plastic threaded part used to slip off when trying to remove the nozzle, leaving the aluminium tip "welded" to the cartridge, forcing us to break it in order to remove it. So, a possible solution could be to find new compatible nozzles, or at best a new bioplotter which resists to higher printing pressures.

3.3 Compression tests

Once the scaffolds were printed, analyses were conducted. They were carried out in Naples, as previously said. Mechanical analysis consisted in compression tests realized on the cylindrical 3D plain PCL and PCL/HA 90/10 (w/w) scaffolds with a 6 mm diameter, 6 mm height and 0°/90° deposition pattern, so to evaluate how hydroxyapatite enhances scaffolds' mechanical properties.

Those tests were conducted using an INSTRON 5566 dynamometer (*Illinois Tool Works Inc, Norwood, MA*), with a 1 mm/min speed and until a 0.5 mm/min deformation was reached

(Figure 3.3). This value corresponds to a 50% deformation, which is way higher than bone's typical deformation levels. It was chosen to have a full material characterization. The dynamometer has two cross-members, an unmovable one and a movable one, which is provided with the load cell. Samples are arranged on the unmovable cross-member, and no hooks are used.

It is important to notice that a scaffold is a porous *structure*. Its characterization is different than a *whole* material one, and that is why we evaluate *compressive modulus*, not Young's modulus. That is because scaffolds' cross section is a *fake* one, due to porosity. Compression tends to make pores smaller, until a whole scaffold is obtained for a 100% deformation. Stress is received by fibers junction, which are resistance points.

Figure 3.3: INSTRON 5566 dynamometer

Measured quantities are *Cauchy stress*, and *compressive modulus*. They were automatically calculated by the Instron software (Bluehill 2, Elancourt, France). To obtain compressive modulus, the software calculates the slope of each stress–strain curve in its elastic deformation region [39].

3.3.1 Results

Compression tests carried out on the plain PCL and PCL/HA 90/10 (w/w) with controlled morphology resulted in the stress/strain curves shown in Figure 3.4. They are characterized by a brief initial elastic region, followed by a non-linear one, until a deformation of 0.5 mm/mm is reached.

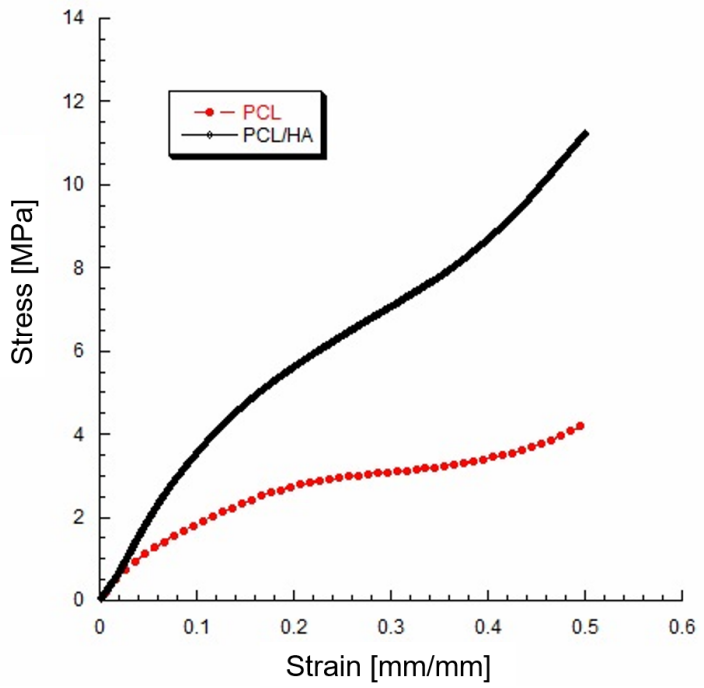

Figure 3.4: Typical stress/strain curves for plain PCL and PCL/HA scaffolds

As expected, our scaffolds' mechanical behaviour resembles any other polymer's one [40]. After a high modulus region, a low stiffness region can be noticed, followed in the end by a region where curve's slope raises. By the way, unlike other polymers, a central *plateau* region, with zero slope, is not present, there is only a region where the slope is lower than the beginning and the end of the curve.

Comparing the two stress/strain curves in the limit displacement value, 0.5 mm/mm, PCL/HA 90/10 (w/w) 3D scaffolds show a higher maximum stress compared to the plain PCL's one: the addition of HA causes hardening in the structure. Plus, compressive modulus, calculated as the curve's initial slope (in the linear region), results higher in PCL/HA scaffolds, meaning that initial compressive stiffness raises. Numerical results are shown in Table 3.2.

Mechanical tests conducted on our samples showed how plain PCL structures are unsatis-

Scaffold	σ_{max} [MPa]	E [MPa]
Plain PCL	4.5 ± 0.6	33.2 ± 3.3
PCL/HA 90/10	11.3 ± 1.4	49.8 ± 5.1

Table 3.2: Maximum stress (σ_{max}) and compressive modulus (E) resulting from the mechanical characterization of the 3D printed scaffolds

fying as scaffolds for orthopedic applications, confirming the need of a structural reinforcement [31].That is why the addition of HA becomes crucial. Hydroxyapatite enhances mechanical performances, hardening the structure through reinforcement particles dispersion inside the polymer matrix [31].

3.4 Biological Analysis: Alamar Blue Assay

As previously seen in paragraph 1.9, hMSCs were seeded on the scaffolds. They are adult stem cells, which can be found inside the bone marrow. They are a good choice for bone tissue engineering, since it has been studied that they contribute to the regeneration of mesenchymal tissues such as bone, cartilage, tendon, etc. [41]. They exhibit plastic adherence and have the ability to differentiate *in vitro* into adipocytes, chondrocytes and osteoblast [42], according to the ECM they detect.

Cells grew into an α -MEM (α-Modified Eagle's Medium, *BioWhittaker, Belgium*), which contains 10% bovine fetal serum, antibiotics (1% penicillin and 1% streptomycin), and 1 μM glutamine. They were put into an incubator (*Forma Scientific, Inc, Marietta, OH*) at 37°C in a 5% CO_2 humidified environment.

After that, those cells were seeded onto our plain PCL and PCL/HA 90/10 scaffolds, $1x10^4$ for each sample, thus obtaining cellular constructs, which were incubated at 37°C to enhance cells adhesion. Scaffolds were previously sterilized in *PenStrep* solution (penicillin and streptomycin) over night. A typical sterilization process consists in a previous UV rays sterilization. However this is a critic process when it comes to scaffolds, because it can harden the polymeric matrix, making the scaffold brittler, thus compromising mechanical behaviour. So, if used, UV rays sterilization must be conveniently modulated.

Biological analysis consists in viability tests, which measure cells vitality and proliferation. They are measured via *Alamar Blue Assay* (*Biosource International, Camarillo, CA*): it is a

sensitive redox (oxidation-reduction) indicator that fluoresces and changes colour upon reduction by living cells [43]. It contains *resazurin*, the reducing substance, the indicator itself, and other substances that prevent an over-reduction to a non-coloured product. When resazurin is oxidized it is red; when it reduces, it becomes resorufin, which is blue. When we refer to Alamar Blue, of course we refer to resazurin.

Alamar Blue's reduction is believed to be mediated by mitochondrial enzymes [44]. It is added to the serum, cells take it into their cytoplasm where it is converted from oxidized to reduced form, thus changing the serum's colour. The coloured product is transported out of the cell and can be measured with a spectrophotometer [12]. Reduction reaction is linked to the living cells number: the stronger the cellular proliferative activity, the more reduced the Alamar Blue will turn. Proliferation and vitality were measured after 1, 3 and 7 days. Right after seeding, and after each measurement, scaffolds were rinsed with PBS (*Sigma-Aldrich, Italy*) and 200 μl of DMEM containing 10% Alamar Blue.

Colouring variation, measured with the spectrophotometer (*UV-Vis, PerkinElmer Lambda 850, PerkinElmer Inc.*) at wavelengths $\lambda = 570$ nm and $\lambda = 595$ nm, is directly proportional to the transformed indicator quantity, and so to the number of viable cells. A solution with *no cells* is used as control. This relation (Equation 3.1) can be found on the Alamar Blue product paper:

$$AlamarBlueReductionRatio = \frac{(O_2 * A_1) - (O_1 * A_2)}{(N_2 * R_1) - (N_1 * R_2)}\% \tag{3.1}$$

where:

- O_1 and O_2 are, respectively, the molar extinction coefficient of oxidized Alamar Blue (Blue) at 570 nm and 595 nm. Their values can be found on the product paper.

- R_1 and R_2 are, respectively, the molar extinction coefficient of reduced Alamar Blue (Red) at 570 nm and 595 nm. Their values can be found on the product paper.

- A_1 and A_2 are, respectively, the absorbance values of test wells at 570 nm and 595 nm.

- N_1 and N_2 are, respectively, the absorbance values of the control wells at 570 nm and 595 nm.

Alamar Blue reduction ratio			
	Day 1	*Day 3*	*Day 7*
PCL-hMSCs	9.3 ± 0.8	14.8 ± 1.5	26.9 ± 2.1
PCL/HA-hMSCs	14.4 ± 1.1	20.1 ± 1.9	34.7 ± 3.5

Table 3.3: Alamar Blue Assay results

3.4.1 Results

Alamar Blue Assay was carried out to evaluate vitality and proliferation of the cells seeded on the 3D polymeric scaffolds in time. In particular, human mesenchymal stem cells (hMSCs) were seeded.

Results are shown in Table 3.3 and graphically in Figure 3.5. Alamar Blue reduction ratio values showed how hMSCs, after 1, 3, and 7 days since seeding, are vital in each sample type. In fact, those values increase with time.

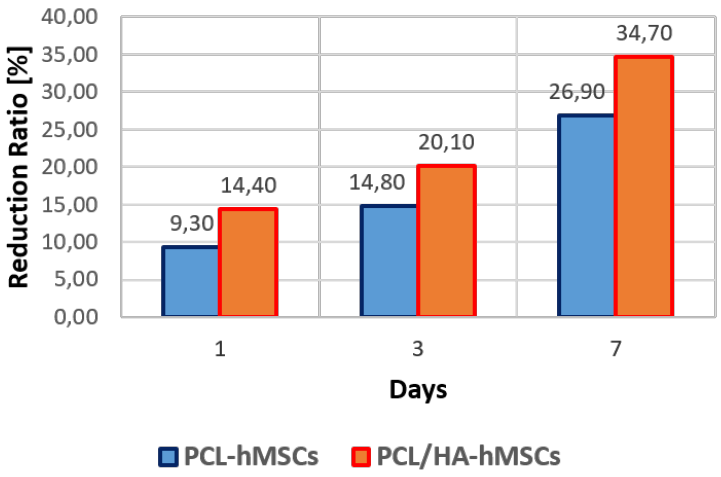

Figure 3.5: Alamar Blue reduction measured for the PCL and PCL/HA scaffolds at 1, 3, and 7 days

PCL/hMSCs cellular constructs showed a lower Alamar Blue reduction ratio than the PCL/HA-hMSCs' one. This means that incorporated reinforcement nanoparticles increase cells vitality and proliferation as well as structure's stiffness, thus resulting in valid orthopedic substitutes for bone tissue engineering. Those results were confirmed by literature sources, where vitality and proliferation increased in reinforced samples as well [12, 31, 32].

Chapter 4

Conclusions and Future Developments

4.1 Conclusions

In this work, cylindrical scaffolds for bone tissue engineering were designed, realized via additive manufacturing techniques, in particular 3D bioprinting, and finally analyzed. Those 3D scaffolds were made of a compound material, a PCL (polycaprolactone) matrix, which mimes bone's ECM organic phase, reinforced with HA (hydroxyapatite) nanoparticles, which actually is part of our bones' ECM mineral phase, in a polymer-to-c. Plain PCL was used to print control scaffolds.

A first and important part of the work consisted in the characterization of PCL printing with our commercial bioplotter, Cellink INKREDIBLE+. In particular, plain PCL (50 kDa and 80 kDa) and PCL/HA 90/10 (w/w) were analyzed. Characterization consisted in the extrusion of material stripes, using different nozzles and pressure/extrusion speed values. Those stripes were then photographed, pre-processed via FIJI and then analyzed thanks to a custom MATLAB script. Results were used to understand the bioprinter's behaviour when it comes to high temperatures and pressures, and to find the best pressure/speed combination that could provide a diameter of 0.3 mm for our strands. Literature parameters were used as a starting point to make the characterization easier. Cellink's PCL was the first one to be characterized. Its results were a starting point for the 80 KDa PCL (the one used in this work), with and without reinforcement. In the end, the 0.3 mm nozzle resulted as the best. An extrusion speed of 45 mm/min was chosen for both materials, while required pressure, as expected, was higher for the reinforced material: that is why 450 kPa was chosen for plain

PCL, and 650 kPa for the reinforced one.

After that, scaffolds realization began. First of all, the compound material was synthesized. The polymer-to-reinforcement weight ratios was 90/10. Synthesis was done in Naples, at the IPCB (Istituto per i Polimeri Compositi e Biomateriali). Then, back to Pavia, scaffolds were designed using SolidWorks, and then the typical pre-printing procedure was carried out. The resulting .stl file was loaded into a slicing software, slic3r, where the .gcode file, a list of coordinates which turn into the printer's printhead trajectories, was created, after printing parameters were set.

For our work and for statistical ends, 23 scaffolds were printed for both PCL/HA 90/10 (w/w) and plain PCL: 8 of them were 6 mm high and were mechanically characterized; the other 15 (2 mm high) were sterilised, and cells were seeded on them for a biological characterization. Both analysis were conducted in Naples.

Mechanical characterization consisted in compression tests. They were carried out using a dynamometer, until a 50% deformation level was reached. Results showed that HA reinforcement enhances the scaffold's mechanical properties, since the PCL alone lacks them.

The 2 mm high scaffolds were sterilised and then human mesenchymal stem cells (hMSCs) were seeded on them. Cells viability was measured thanks to the Alamar Blue Assay. Alamar Blue is a redox indicator which changes colour when it passes from oxidized to reduced form. Its reduction depends on the number of living cells. Results showed that viability was higher on the reinforced samples, thus confirming that the HA reinforcement enhances cells vitality and proliferation too.

This work opened the gates to a lot of future works. It was a pilot study, so our results are preliminary, and most of the work consisted in verifying their consistency, compared to literature ones.

4.2 Future Developments

Future developments of this study deal with material, scaffold and biological aspects.

- Material developments: as our literature review showed, compound materials for bone tissue engineering are various. PCL's molecular weight can vary, thus varying its density, its mechanical properties, and cells proliferation; reinforcement can vary as well: it can be hydroxyapatite in different concentrations, so to show how the increasing of HA nanoparticles enhances mechanical properties more than our results, until a critic concentration is reached (circa 70%). From then, HA nanoparticles act as weak points, even though biological properties may increase. This means that there is a trade-off between mechanical and biological enhancement, and that is why future research will deal with 3D nanocomposite scaffolds realized after a topological optimization process. Other materials can be used as reinforcement, such as calcium and carbon nanotubes, and similar tests can be conducted.

- Scaffold developments: porosity depends on strand distance and layers orientation. If those parameters vary, pores dimensions and geometry will vary as well, thus allowing further analysis involving different cells. Scaffold geometry, on the other hand, can influence mechanical behaviour.

- Biological developments: there are a lot of possible ways to proceed for biological investigations. Further analysis can be done, for example carrying out differentiation tests on the scaffolds, thus verifying if hMSCs differentiate into bone's cell types. Plus, we seeded hMSCs on our scaffolds, but osteoblasts or osteocytes can be seeded as well.

Bibliography

[1] A Gloria, T Russo, R De Santis, and L Ambrosio. 3d fiber deposition technique to make multifunctional and tailor-made scaffolds for tissue engineering applications. *Journal of Applied Biomaterials & Biomechanics*, 7(3), 2009.

[2] Wikimedia Commons. https://commons.wikimedia.org.

[3] J Groll, T Boland, T Blunk, J A Burdick, D Cho, PD Dalton, B Derby, G Forgacs, Q Li, A M, Vladimir, et al. Biofabrication: reappraising the definition of an evolving field. *Biofabrication*, 8(1):013001, 2016.

[4] M Neufurth, X Wang, S Wang, R Steffen, M Ackermann, ND Haep, HC Schröder, and WEG Müller. 3d printing of hybrid biomaterials for bone tissue engineering: Calcium-polyphosphate microparticles encapsulated by polycaprolactone. *Acta biomaterialia*, 64:377–388, 2017.

[5] M Domingos, F Intranuovo, T Russo, R De Santis, A Gloria, L Ambrosio, J Ciurana, and P Bartolo. The first systematic analysis of 3d rapid prototyped poly (ε-caprolactone) scaffolds manufactured through biocell printing: the effect of pore size and geometry on compressive mechanical behaviour and in vitro hmsc viability. *Biofabrication*, 5(4):045004, 2013.

[6] RepRap Website. http://reprap.org.

[7] Cellink Website. https://cellink.com/.

[8] PEMF Therapy Website. https://www.pemftherapyeducation.com.

[9] CLM Bao, EY Teo, MSK Chong, Y Liu, M Choolani, and JKY Chan. Advances in bone tissue engineering. In *Regenerative Medicine and Tissue Engineering*. InTech, 2013.

[10] Istituto Gobetti Website. http://www.istitutogobetti.it.

[11] MOLTENO Website. https://www.molteno.com.

[12] A Gloria, T Russo, U D'Amora, S Zeppetelli, T D'Alessandro, M Sandri, M Bañobre-López, Y Piñeiro-Redondo, M Uhlarz, Anna Tampieri, et al. Magnetic poly (ε-caprolactone)/iron-doped hydroxyapatite nanocomposite substrates for advanced bone tissue engineering. *Journal of The Royal Society Interface*, 10(80):20120833, 2013.

[13] MS Chapekar. Tissue engineering: challenges and opportunities. *Journal of Biomedical Materials Research Part A*, 53(6):617–620, 2000.

[14] JP Vacanti and R Langer. Tissue engineering: the design and fabrication of living replacement devices for surgical reconstruction and transplantation. *The lancet*, 354:S32–S34, 1999.

[15] R Cancedda, P Giannoni, and M Mastrogiacomo. A tissue engineering approach to bone repair in large animal models and in clinical practice. *Biomaterials*, 28(29):4240–4250, 2007.

[16] A Gloria, R De Santis, and L Ambrosio. Polymer-based composite scaffolds for tissue engineering. *Journal of Applied Biomaterials & Biomechanics*, 8(2), 2010.

[17] G Vaissiere, B Chevallay, D Herbage, and O Damour. Comparative analysis of different collagen-based biomaterials as scaffolds for long-term culture of human fibroblasts. *Medical and Biological Engineering and Computing*, 38(2):205–210, 2000.

[18] F Causa, PA Netti, and L Ambrosio. A multi-functional scaffold for tissue regeneration: the need to engineer a tissue analogue. *Biomaterials*, 28(34):5093–5099, 2007.

[19] DW Hutmacher, M Sittinger, and MV Risbud. Scaffold-based tissue engineering: rationale for computer-aided design and solid free-form fabrication systems. *TRENDS in Biotechnology*, 22(7):354–362, 2004.

[20] HK Kleinman, D Philp, and MP Hoffman. Role of the extracellular matrix in morphogenesis. *Current opinion in biotechnology*, 14(5):526–532, 2003.

[21] E Sachlos, JT Czernuszka, et al. Making tissue engineering scaffolds work. review: the application of solid freeform fabrication technology to the production of tissue engineering scaffolds. *Eur Cell Mater*, 5(29):39–40, 2003.

[22] PJ Bartolo and J Gaspar. Metal filled resin for stereolithography metal part. *CIRP Annals-Manufacturing Technology*, 57(1):235–238, 2008.

[23] J Zuniga, D Katsavelis, J Peck, J Stollberg, M Petrykowski, A Carson, and C Fernandez. Cyborg beast: a low-cost 3d-printed prosthetic hand for children with upper-limb differences. *BMC research notes*, 8(1):10, 2015.

[24] F Guillemot, V Mironov, and M Nakamura. Bioprinting is coming of age: report from the international conference on bioprinting and biofabrication in bordeaux (3b'09). *Biofabrication*, 2(1):010201, 2010.

[25] JD Currey. The structure of bone tissue. *Bones: Structure and mechanics*, page 3r26, 2002.

[26] MA Woodruff and DW Hutmacher. The return of a forgotten polymer—polycaprolactone in the 21st century. *Progress in polymer science*, 35(10):1217–1256, 2010.

[27] P Zheng, Q Yao, F Mao, N Liu, Y Xu, B Wei, and L Wang. Adhesion, proliferation and osteogenic differentiation of mesenchymal stem cells in 3d printed poly-ε-caprolactone/hydroxyapatite scaffolds combined with bone marrow clots. *Molecular medicine reports*, 16(4):5078–5084, 2017.

[28] D Buser, C Dahlin, and RK Schenk. Guided bone regeneration. *Chicago Quintessence*, 1994.

[29] G Ciapetti, L Ambrosio, L Savarino, D Granchi, E Cenni, N Baldini, S Pagani, S Guizzardi, F Causa, and A Giunti. Osteoblast growth and function in porous poly ε-caprolactone matrices for bone repair: a preliminary study. *Biomaterials*, 24(21):3815–3824, 2003.

[30] D Rohner, DW Hutmacher, TK Cheng, M Oberholzer, and B Hammer. In vivo efficacy of bone-marrow-coated polycaprolactone scaffolds for the reconstruction of orbital defects

in the pig. *Journal of Biomedical Materials Research Part B: Applied Biomaterials*, 66(2):574–580, 2003.

[31] F Causa, PA Netti, L Ambrosio, G Ciapetti, N Baldini, S Pagani, D Martini, and A Giunti. Poly-ε-caprolactone/hydroxyapatite composites for bone regeneration: In vitro characterization and human osteoblast response. *Journal of Biomedical Materials Research Part A*, 76(1):151–162, 2006.

[32] SA Park, SH Lee, and WD Kim. Fabrication of porous polycaprolactone/hydroxyapatite (pcl/ha) blend scaffolds using a 3d plotting system for bone tissue engineering. *Bioprocess and biosystems engineering*, 34(4):505–513, 2011.

[33] B Kim, S Yang, and J Lee. A polycaprolactone/cuttlefish bone-derived hydroxyapatite composite porous scaffold for bone tissue engineering. *Journal of Biomedical Materials Research Part B: Applied Biomaterials*, 102(5):943–951, 2014.

[34] J Ródenas-Rochina, JLG Ribelles, and M Lebourg. Comparative study of pcl-hap and pcl-bioglass composite scaffolds for bone tissue engineering. *Journal of Materials Science: Materials in Medicine*, 24(5):1293–1308, 2013.

[35] EM Gonçalves, FJ Oliveira, RF Silva, MA Neto, MH Fernandes, M Amaral, M Vallet-Regí, and M Vila. Three-dimensional printed pcl-hydroxyapatite scaffolds filled with cnts for bone cell growth stimulation. *Journal of Biomedical Materials Research Part B: Applied Biomaterials*, 104(6):1210–1219, 2016.

[36] V Guarino, F Veronesi, M Marrese, G Giavaresi, A Ronca, M Sandri, A Tampieri, M Fini, and L Ambrosio. Needle-like ion-doped hydroxyapatite crystals influence osteogenic properties of pcl composite scaffolds. *Biomedical Materials*, 11(1):015018, 2016.

[37] P Bartolo, M Domingos, A Gloria, and J Ciurana. Biocell printing: Integrated automated assembly system for tissue engineering constructs. *CIRP Annals-Manufacturing Technology*, 60(1):271–274, 2011.

[38] P Sheshadri. *Characterization of 3D-Bioplotting of ϵ-Polycaprolactone for Tissue Engineering Applications*. PhD thesis, North Carolina State University, 2014.

[39] F Croisier, AS Duwez, C Jérôme, AF Léonard, KO Van Der Werf, PJ Dijkstra, and ML Bennink. Mechanical testing of electrospun pcl fibers. *Acta biomaterialia*, 8(1):218–224, 2012.

[40] I Engelberg and J Kohn. Physico-mechanical properties of degradable polymers used in medical applications: a comparative study. *Biomaterials*, 12(3):292–304, 1991.

[41] MF Pittenger, AM Mackay, SC Beck, RK Jaiswal, R Douglas, J D Mosca, MA Moorman, DW Simonetti, S Craig, and DR Marshak. Multilineage potential of adult human mesenchymal stem cells. *science*, 284(5411):143–147, 1999.

[42] I Ullah, RB Subbarao, and GJ Rho. Human mesenchymal stem cells-current trends and future prospective. *Bioscience reports*, 35(2):e00191, 2015.

[43] R Hamid, Y Rotshteyn, L Rabadi, R Parikh, and P Bullock. Comparison of alamar blue and mtt assays for high through-put screening. *Toxicology in vitro*, 18(5):703–710, 2004.

[44] J O'brien, I Wilson, T Orton, and F Pognan. Investigation of the alamar blue (resazurin) fluorescent dye for the assessment of mammalian cell cytotoxicity. *The FEBS Journal*, 267(17):5421–5426, 2000.

Ringraziamenti

Durante questo mio lavoro di tesi tra Pavia e Napoli, l'aiuto di alcune persone mi è stato molto prezioso: mi sembra doveroso ringraziarle tutte.

Innanzitutto voglio ringraziare il mio relatore, il professor Michele Conti, che da subito si è dimostrato molto disponibile e mi ha fornito gli stimoli e la grinta giusta per affrontare questo lavoro, e il Professore Ferdinando Auricchio, senza il quale questa collaborazione e questo lavoro non esisterebbero. Restando a Pavia, il ringraziamento più grande va sicuramente alla Dottoressa Franca Scocozza, che mi ha seguito per tutta la durata del lavoro, con tanta pazienza e dedizione. Un grazie anche all'Ingegnere Stefania Marconi, il cui aiuto è stato fondamentale nel momento del design e della stampa degli scaffold.

Passando a Napoli, il ringraziamento più importante è per il Professore Antonio Gloria, presenza e guida costante nel mio percorso universitario, che ha saputo farmi appassionare a questa grande scienza. Grazie alla Dottoressa Teresa Russo e alla Dottoressa Olimpia Oliviero, il cui aiuto è stato prezioso in fasi cruciali del lavoro.

Ovviamente, devo ringraziare anche tante persone che mi hanno supportato e che hanno fatto il tifo per me: il primo ringraziamento è per la mia famiglia e per Rossella, che è sempre stata al mio fianco e mi ha impedito di fare tanti passi falsi. Grazie a tutti i miei amici e colleghi, e in particolare a Bruna, che è stata una compagna di viaggio perfetta per questo percorso universitario.